ORNL/TM-2022/2752

Oak Ridge National Laboratory: Additive Manufacturing Design Guidelines for Wind Industry

Amiee Jackson
Celeste Atkins
Abigail Barnes
Vidya Kishore
Brian Post
Christopher Hershey
Michael Borish
Halil Tekinalp
Alex Roschli
Phillip Chesser
Tyler Smith
Pum Kim
Vlastimil Kunc
Lonnie Love
David Snowberg*
Scott Carron*

October 2022

ORNL IS MANAGED BY UT-BATTELLE LLC FOR THE US DEPARTMENT OF ENERGY

*associated with NREL

ORNL/TM-2022/2752

Energy Transportation Sciences Directorate
Manufacturing Sciences Division

ADDITIVE MANUFACTURING DESIGN GUIDELINES FOR WIND INDUSTRY

Authors:
Amiee Jackson
Celeste Atkins
Abigail Barnes
Vidya Kishore
Brian Post
Christopher Hershey
Michael Borish
Halil Tekinalp
Alex Roschli
Phillip Chesser
Tyler Smith
Pum Kim
Vlastimil Kunc
Lonnie Love
David Snowberg*
Scott Carron*

October 2022

Prepared by
OAK RIDGE NATIONAL LABORATORY
Oak Ridge, TN 37831
managed by
UT-BATTELLE LLC
for the
US DEPARTMENT OF ENERGY
under contract DE-AC05-00OR22725

CONTENTS

LIST OF FIGURES

LIST OF TABLES

ABBREVIATIONS

3DP	3D printing
3DSP	3D sand printing
ABS	acrylonitrile butadiene styrene
AM	additive manufacturing
BAAM	big area additive manufacturing
BJ	binder jetting
CAM-LEM	computer aided manufacturing of laminated engineering materials
CBAM	composite based additive manufacturing
CF	carbon fiber
C-FAB	cellular fabrication
CIM	ceramic injection molding
CLIP	continuous liquid interface production
CNC	computer numerical control
CNC	cellulosic nanocrystals
CNF	carbon nanofibers
CTE	coefficient of thermal expansion
DED	directed energy deposition
DLP	digital light processing
DMLM	direct metal laser melting
DMLS	direct metal laser sintering
DOD	drop-on-demand
DPI	dots per inch
EBAM	electron beam additive manufacturing
EBM	electron beam melting
FDM	fused deposition modeling
FFF	fused filament fabrication
GF	glass fiber
HGM	hollow glass microspheres
HIP	hot isostatic pressing
LDW	laser deposition welding
LENS	laser engineered net shaping
LMD	laser metal deposition
LOM	laminated object manufacturing
mBAAM	metal big area additive manufacturing
ME	material extrusion
MIM	metal injection molding
MJM	multi-jet modeling
MVP	Magnum Venus Products
NPJ	nanoparticle jetting
ORNL	Oak Ridge National Laboratory
PBF	powder bed fusion
PBS	polybutylene succinate
PET	polyethylene terephthalate
PETG	polyethylene terephthalate glycol
PLA	polylactic acid
PPS	polyphenylen sulfide
PPSU	polyphenylsulfone

PS	polystyrene
PSL	plastic sheet lamination
PSU	polysulfone
SHS	selective heat sintering
SL	sheet lamination
SLA	stereolithography (process)
SLCOM	selective lamination composite object manufacturing
SLM	selective laser melting
SLS	selective laser sintering
STL	stereolithography (file format)
TPU	thermoplastic polyurethane
UAM	ultrasonic additive manufacturing
VP	vat photopolymerization
WAAM	wire arc additive manufacturing

ABSTRACT

The purpose of this report is to equip wind industry professionals with the fundamental information needed to best leverage additive manufacturing techniques in their design and manufacturing decisions. Over the past 10 years, wind turbine ratings have increased from a typical 3MW turbines in the early 2010's to General Electric's Haliade-X 12-13MW and Siemens Gamesa's 14MW turbines developed in 2019-2021 [1]. Turbine ratings increase by building taller towers with larger swept areas, meaning longer blades and more robust structural components in the rotor and nacelle. For example, hub masses for 3MW turbines have been reported around 20-30 metric tonnes, while hub masses for 10-15MW turbines have been reported around 100-190 metric tonnes [2-6]. Looking to the future, literature shows intention to design turbines rated for 20-50MW and beyond, particularly in the offshore wind market [1, 7-10]. As the size and quantity of wind turbine structures increase with time, designers face mounting manufacturing obstacles, such as limited supply chain for large castings like bedplates and hubs or time and labor-intensive manufacturing processes in composite layup structures such as blades or nacelle covers. Manufacturing challenges for wind turbine components such as blade structures or large castings within the nacelle and rotor may be met with advanced manufacturing methods and techniques like additive manufacturing. Herein an overview of each of the seven families of additive manufacturing is provided, along with typical materials used in each process, current ranges on process speeds, materials and system costs, and examples of systems on the market today. Using the lens of large-scale additive to suit the needs of the wind industry, the processes that are well-suited to large-scale production are down selected from the seven families and additional information with design guidelines specific to each process are detailed. A companion document titled "Relevant Additive Manufacturing Materials for Wind Industry" elaborates on the specifics of relevant material properties and test methods for additive manufacturing materials.

1. INTRODUCTION

Additive Manufacturing (AM), also known as 3D printing, has been around since the 1980s with the invention of stereolithography (SLA) [11]. Since then, many more additive processes have been developed. These processes are grouped into one of seven distinct families of AM: vat photopolymerization (which includes SLA), powder bed fusion, binder jetting, material jetting, sheet lamination, material extrusion (which includes FDM), and directed energy deposition [11]. Each of these families, and each AM process, is distinguished by a unique way of constructing an object, as shown in Figure 1. One commonality, however, is that they all take a layer-based approach.

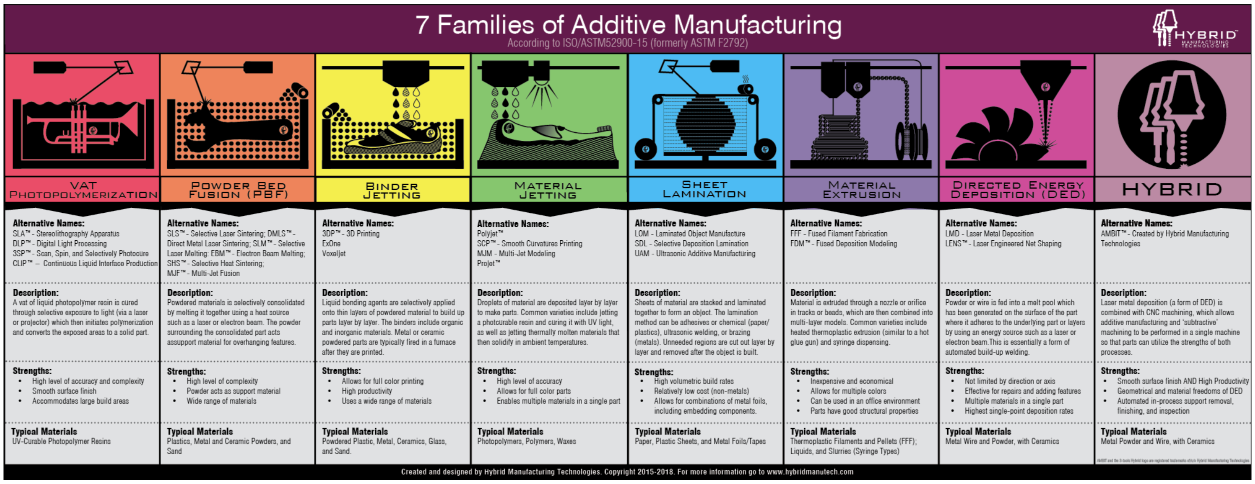

Figure 1. The seven families of additive manufacturing, as defined by Hybrid Manufacturing Technologies [12]. Note: hybrid processes indicate a blend of additive and subtractive methods to produce a part.

A generalized process flow for all AM families consists of design, pre-processing, production, post-processing, testing, and end use. Decisions made at each process flow step, including process and material selection, processing parameters, finishing processes, and certification testing, are directly related to the end use of the object: its form, fit, and function.

The pre-processing step transforms a CAD model into machine-specific toolpaths for production. Typically, a CAD design file is converted into an STL file. The STL file format, common across the industry, represents a CAD model's geometry with triangular faceted surfaces. A process or machine-specific slicing program is then used to select the part's position, scale, and orientation within the print volume; to select process parameters; and to calculate the toolpaths necessary to fabricate the part. This program is referred to as a slicer because it programmatically slices the three-dimensional geometry into a stacked set of two-dimensional cross-sections, or layers [11]. The output of the slicer is machine-specific, part-specific code that automates the production process.

Production processes in AM execute the code output from the slicing program. The two-dimensional cross-sections are constructed sequentially, layer-by-layer, by leveraging one of the seven fundamental process families of AM, described in the following section.

2. THE SEVEN FUNDAMENTAL ADDITIVE MANUFACTURING FAMILIES

2.1 VAT PHOTOPOLYMERIZATION

Vat photopolymerization is defined in ASTM F2792 [13] as "an additive manufacturing process in which liquid photopolymer in a vat is selectively cured by light-activated photopolymerization". A photocatalytic curing process is used to grow components from a vat of photo-sensitive thermoset liquid. This process uses UV curable photopolymers and boasts fine feature resolution and excellent surface finish, with typical layer thicknesses of 0.05-0.15mm [14-16]. Interlaminar strength is limited by oxygen inhibition which creates a dead-zone where the resin will not cure [16]. After a part is built, post-processing includes washing, removing support structures, and a second curing. It should be noted that there are significant safety issues associated with chemical handling of many resins, as some have been known to cause cancer [17]. Because the size of the vat limits the maximum volume of material that can be processed, build sizes less than $0.02m^3$ are most common. One of the largest machines for this process was built specifically for prototyping dashboards in vehicles, with a build volume of 1.5m x 0.75m x

0.55m [18]. Typical build rates are in the 5-10in^3/hr range, although some process variants (i.e. DLP or CLIP) allow for faster build rates which are limited by resin cure rates and viscosity rather than laser scan rates. Where traditional SLA printers have vertical print speeds of a few millimeters per hour, vertical print speeds on CLIP may approach hundreds of millimeters per hour. These process rates are expressed in two different ways (volumetric speed vs vertical speed) due to the nature of each process type. Typical SLA printers process material in a point-wise fashion, which means that the area of each layer governs the vertical print speed (coupled with the spot size and linear scanning speed). DLP and CLIP printers process material in an area-wise fashion, which means that the area of each layer is not coupled to the vertical print speed. Thus, in theory a significantly higher volumetric print rate could be achieved using this technology [16]. Two drawbacks of the photopolymers used are their feedstock unit price, which is very high in comparison to feedstock materials in other AM processes ($100's/kg), and their limited mechanical performance, which can degrade over time with exposure to UV. This time-related mechanical performance is due to continued curing of the photopolymer which leads to embrittlement. Thus, one fundamental limitation to the process is achieving just the level of curing desired for peak mechanical properties—not too much, not too little. Processes such as stereolithography (SLA), digital light processing (DLP), and continuous liquid interface production (CLIP) fall into the vat photopolymerization family. Common industry applications include hearing aids and dentistry, as custom and high resolution parts are required while strength properties are not as critical. Other applications may include patterns for vacuum casting, sacrificial patterns for metal casting, short-run production injection mold tools, wind tunnel models, custom assembly jigs or fixtures, tools, molds, and dies [18].

2.2 MATERIAL JETTING

Material jetting is defined in ASTM F2792 [13] as "an additive manufacturing process in which droplets of build material are selectively deposited." Here, an array of inkjet printheads on a shared carrier simultaneously deposit and solidify material in a linear fashion, similar to the standard 2D ink jetting process [19]. Post processing includes removal of support material and in some cases a second curing cycle. Materials including photopolymers, metals, and waxes can be deposited in this manner [20]. Some variants of this process type also use thermoplastics, ceramics, or biomaterials. Waxes can be used for precision investment casting. As thermoset photopolymer resins are jetted and cured in place, multi-material and graded material parts (termed "digital materials") are feasible when multiple inkjets with different materials are used. Dots per inch (dpi) gradients can be leveraged to transition material Durometers, Shore hardness, or colors for unique part functionality and aesthetic [19]. These processes boast high dimensional accuracy, excellent surface finish, and a low risk of warping, with layer heights as low as 13µm [19, 21, 22]. Resolution in XY may be as fine as 600 dpi, with 1600 dpi in Z [19, 23]. The major limiting factor to process scalability is the unit price of feedstock materials, which is quite high ($100's/kg) for both wax materials and thermosets [24, 25]. Technical challenges for this process include materials selection, machine reliability, and part consistency [19]. Vertical build rates are typically in the 10's mm/hr, with volumetric rates of 10's cc/hr [23, 26]. A variety of materials may be used in this type of process, so long as the material is ink-jettable (determined by viscoelastic properties, specifically the Ohnesorge number) [19]. One advantage to this process is that there is almost no wasted material as compared to vat photopolymerization. Large build sizes reach 0.4m^3, but typical build sizes are closer to 0.02m^3. Processes such as drop-on-demand (DOD), multi-jet modeling (MJM), PolyJet, and nanoparticle jetting (NPJ) fall into the material jetting family. Future developments in material jetting include tunable structures via "smart materials", printed hybrid electronics, and new jettable inks [19]. Common industry applications include dentistry, medical models, and prototypes for photopolymers, while waxes have been used for direct investment casting. Other applications for photopolymers may include short-run production injection mold tools.

2.3 BINDER JETTING

Binder jetting is defined in ASTM F2792 [13] as "an additive manufacturing process in which a liquid bonding agent is selectively deposited to join powder media." Thin layers of powder are spread over the print bed, followed by binder deposition via inkjet printheads. The print bed lowers after each layer, allowing the following layer of powder to be spread. After all layers of deposition are completed, a fragile "green" part is cured (aka de-bound) in the powder reservoir yielding a "brown" part. Next, it is cleaned from the powder reservoir and typically must be post-processed via infiltration and/or sintering to realize its full strength [27]. Common powder materials in binder jetting include ceramics (glass, gypsum, sandstone), sand, and metals [28]. Other materials include biomaterials, sugar, plaster, and pharmaceuticals [20, 26]. Sand typically does not require post-processing in a furnace, while other materials do. While the materials library for these processes is expansive, the cost of sand ($100's/ton) is orders of magnitude less than that of metals ($100's/lb) [29, 30]. Binder materials can be categorized by application: furan binder for sand casting, phenolic or silicate binder for sand molds and cores, and aqueous-based binder for metals [20, 31]. Overall, binder jetting requires no support structure, is highly dimensionally accurate, and presents a low risk of warping or distortion. However, green parts that undergo sintering shrink as the binder burns off. This shrinkage creates challenges for geometric control as different geometries will shrink differently. A typical minimum feature size associated with binder jetting is about 0.1mm [32]. There is a fundamental limit to the minimum powder particle size at about 20µm, which limits resolution [32]. For metal parts, infiltration with a lower melting point alloy is commonly leveraged to decrease end part porosity [27]. Another advantage of binder jetting processes is the potential to utilize the full build volume throughout a print for parallel production of many different parts, thus improving machine efficiency. However, 20% part packing density is considered a highly optimized build. When comparing to other AM processes, binder jetting also offers the cost benefit of divorcing the cost and processing rate from the part geometry. For parts that require sintering, multiple sections can be printed separately and joined in the furnace. Typical build rates are around 100cc/hr, with some systems claiming capabilities up to 125,000cc/hr [26, 33, 34]. It should be noted, however, that these rates do not account for the de-binding, sintering, cleaning, and other post-processing steps. De-powdering time is highly geometry dependent, but has typically been seen to take around 20% of the print time. Large build volumes in the range of $8m^3$ are seen [26], particularly with sand or stone, while ceramics and metals typically range from $0.01m^3$ to $0.16m^3$. As a benchmark, the cost of an ExONE S-Max Pro with 2 job boxes was $1.35 million in April 2021. To contract a build for the full volume (1800mm x 1000mm x 700mm) would be $10,700. One major advantage is the ability to reuse or reclaim nearly all of the waste powder from the process, as there are no thermal effects which might compromise the powder morphology. Systems and processes that fall into the binder jetting family include MIT's 3DP, ExOne, 3D sand-printing (3DSP), and metal jet fusion. Future innovations in this family include optimized binder development and methods to improve final mechanical properties of metal parts. Leverage of binder jetting for sand molds holds promise for reduction of design integration times, decreased production time, and adaptability to design changes. Sand mold production with binder jetting expands geometric flexibility when compared to other production methods, allowing for small features, complex curvature, and internal cavities.

Figure 2: ExOne's S-MAX Pro is a commercially available example of an industrial scale 3DSP machine. Source: https://www.3dprintingmedia.network/wp-content/

Figure 3: D-shape's large-scale binder jetting machine. Source: https://3dprintingindustry.com/

Figure 4: Desamanera's large-scale binder jetting machine uses stone blends as feedstock. Source: https://www.desamanera.com/

Figure 5: Z-Corp's Z510 is one of the oldest examples of a classic binder jetting machine. Source: https://www.treatstock.com/

Figure 6: HP's Metal Jet printer is the quintessential example of metal jetting technology.
Source: https://store.hp.com/app/

2.4 POWDER BED FUSION

Powder bed fusion (PBF) is defined in ASTM F2792 [13] as "an additive manufacturing process in which thermal energy selectively fuses regions of a powder bed." This follows a similar vein as binder jetting but uses an intense energy source to melt or sinter powder rather than a binding agent. In the process, a thin layer of powder is spread over the print bed before a laser or e-beam selectively sinters or melts the powder. Then the print bed lowers for the following layer of powder to be spread. Polymer, metal, and ceramic materials are processed with high spatial resolution, excellent surface finish, and nearly complete densification of an end part. Resolution achieved with e-beam processes is worse than that achieved with laser processes [35, 36]. However, process rate achieved with e-beam processes outpaces that achieved with laser processes [37]. Typical metals used in this process type include high-value alloys such as: titanium, inconel, tungsten, tantalum, cobalt chrome, copper, etc. Post-processing for this family may include HIP for stress-relief and machining for key mating surfaces. High-vacuum environments in the build chamber are required for e-beam processes. The process can yield residual stress issues, particularly when a laser energy source is used. These residual stresses may result in part failure due to collision between the recoater and a deformed or warped part [37]. Powdered feedstock materials are expensive ($100's/kg) [29], but material that has not been melted can be blended with virgin material to be recycled in many cases. Polymer processes typically reclaim about 20% of the unmelted powder, which leaves a significant volume as waste material. However, metal processes often reclaim 50-80% of unmelted powder. Major limitations to process scalability include the requirement for inert environment, the unit price of feedstock material, and the overall relatively slow process rates. Typical deposition rates are around 10-15in^3/hr, with some systems boasting up to 300in^3/hr. The process rate is typically limited by how quickly the energy source can be scanned across a layer, or how quickly a layer can be recoated [37, 38]. There are also physical bounds to process rate due to carbonization, vaporization or soot production at high energy densities [37]. Build volumes up to 0.5m^3 are seen, although the typical volume remains around 0.02m^3. A major limitation to build volume is powder safety: as powders are highly flammable, there are limitations to what volume of powder can be stored at any given point in time. Additionally, there are a number of safety considerations that must be taken into account for powder handling (i.e. respirators). Processes such as direct metal laser sintering (DMLS), direct metal laser melting (DMLM), electron beam melting (EBM), selective heat sintering (SHS), selective laser melting (SLM) and selective laser sintering (SLS) fall into the powder bed fusion family. Future innovations in this family include microstructure control, methods to further decrease part porosity, and multi-laser sources to increase process rates. Overall, the total cost of this process must be underscored, with major contributors including machine amortization, service contracts, utilities required for environmental controls, labor, feedstock material, and post-processing. When accounting for total cost, the material feedstock cost may comprise 1/3 of the total cost or less [29, 37].

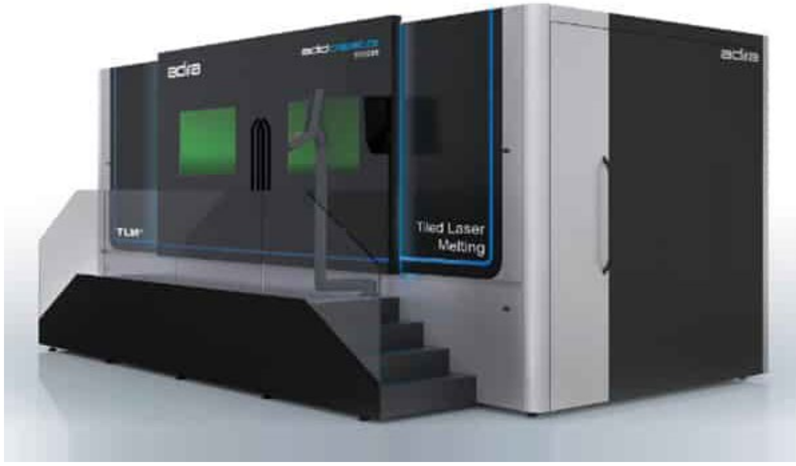

Figure 7: Adira's AddCreator machine leverages tiled laser melting (TLM) to push PBF processes to larger scale manufacturing.
Source: https://www.aniwaa.com/

Figure 8: The SLM 800 machine features SLM Solution's largest build volume yet.
Source: https://www.slm-solutions.com/

2.5 DIRECTED ENERGY DEPOSITION

Directed energy deposition (DED) is defined in ASTM F2792 [13] as "an additive manufacturing process in which focused thermal energy is used to fuse materials by melting as they are being deposited." This process constructs a part by using an intense energy source, such as a laser, electron beam or plasma arc, to selectively melt a coaxial metal feedstock, in the form of wire or powder. Although most applications use metal, other materials such as polymers, ceramics, and composites can be similarly processed. Wire feedstock is typically about ½ the cost of powder feedstock for a given material, and has shorter lead times [39]. Feedstock cost is highly dependent on the material: stainless steel 316 wire runs around $2-5/lb, while powder runs around $10/lb [39]. Ti-6Al-4V, on the other hand, runs around $50/lb while powder runs around $120/lb [39]. When accounting for total process cost, however, the unit price of this process increases substantially due to machine amortization, labor, utilities required for environmental controls, and post-processing. This process family fundamentally differs from powder bed fusion because the feedstock material is selectively deposited only in the path of the energy source. Substantial crossover between DED processes and welding techniques allows DED applications to expand beyond part creation to include repair, remanufacturing, and surface coating. DED processes can engineer material composition and property gradients in large-scale parts, positioning them with a high potential impact. Typical deposition rates range between 5-25lb/hr, with little material waste [39]. Powder-based DED processes have deposition rates on the lower end of this range (up to 5 lb/hr), while multi-wire electron beam-based processes dominate the high end. However, residual stress accumulation in parts, due to large thermal gradients, can result in distortion and require additional processing steps to relieve stresses such as HIP. Additionally, a shielding gas or an inert environment is often required to prevent oxidation. DED processes are often combined with subtractive processes in hybrid manufacturing, or parts are manufactured to near-net-shape in the additive process and machined to tolerance in post-processing. Build volumes on the order of multiple cubic meters are seen, particularly when using wire as feedstock. Processes such as laser deposition welding (LDW), electron beam additive manufacturing (EBAM), laser metal deposition (LMD), laser engineered net shaping (LENS), wire arc additive manufacturing (WAAM), and wire feed metal additive manufacturing fall into the directed energy deposition family. Future innovations in this family include hybrid manufacturing, microstructure control, and large-scale parts.

Figure 9: RAMLAB's WAAM configuration has spearheaded large scale part production in the DED space. Source: https://www.additivemanufacturing.media/news/consortium-builds-ship-propeller-via-wire-plus-arc-additive-manufacturing-waam-

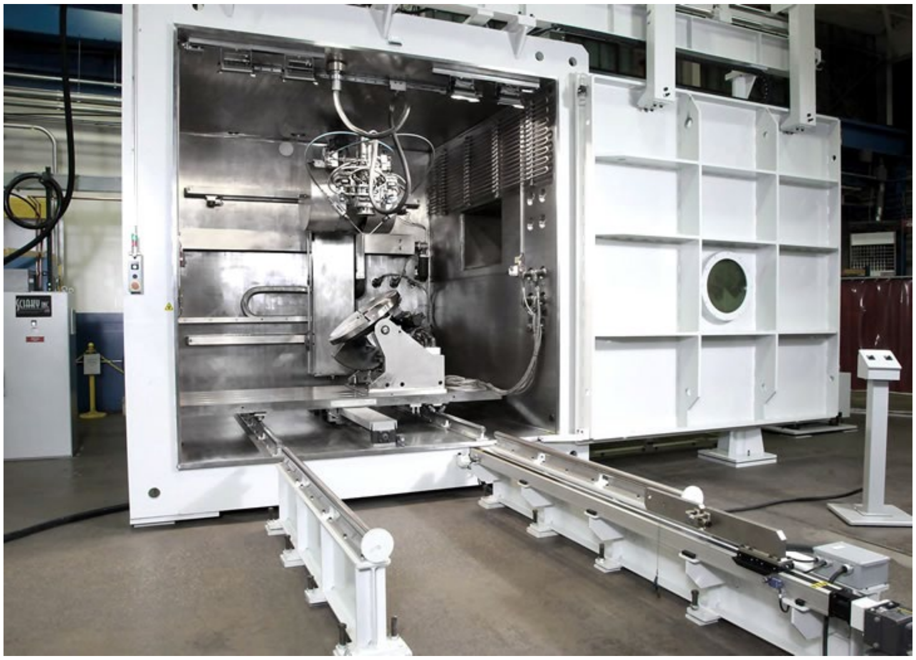

Figure 10: Sciaky's Electron Beam Additive Manufacturing (EBAM) process.
Source: https://additivemanufacturing.com/

Figure 11: Optomec's LENS CS 800 Additive utilizes their LENS process.
Source: https://optomec.com/

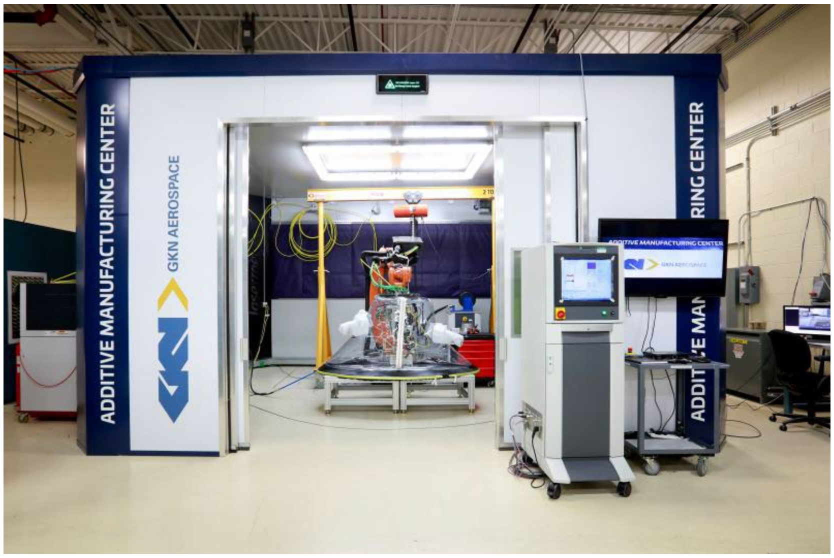

Figure 12: GKN Aerospace's LMD-w cell is under active development at ORNL's MDF. Source: https://3dprintingindustry.com/

2.6 MATERIAL EXTRUSION

Material extrusion is defined in ASTM F2792 [13] as "an additive manufacturing process in which material is selectively dispensed through a nozzle or orifice." This forces feedstock material through an orifice to form a bead while traversing the path of a layer. Although thermoplastic polymers are the most common materials used, foams [40, 41], thermosets [42], composites [43, 44], and paste-like materials such as chocolate, concrete [28, 45], or clay-based materials are also processed in this manner. Highly filled polymer formulations with metals or ceramics further expand the potential applications of material extrusion products [46]. Extruder mechanisms vary and can include feed rollers, extrusion screws [47] or augers, and rams or plungers [46]. ME processes are capable of multi-material and functionally graded material production [48]. Surface finish is generally correlated to total build size due to the economics of processing time; that is, as build size increases, surface finish and minimum feature size deteriorate. Mechanical properties are generally anisotropic due to limitations in interlaminar adhesion [49]. For polymer-based systems, feedstocks at the small scale are typically filaments ($10's-100's/lb), which when scaled up are not economically feasible for large scale. However, pellet-based feedstocks ($1's-10's/lb) are used at the large scale to address this unit-cost issue [50]. The BAAM system can achieve build rates of 60 lb/hr, while mid-size systems like that of 3DP achieve rates around 15 lb/hr. Desktop scale polymer systems typically achieve build rates of 30-90 cc/hr [26]. Processes such as fused deposition modeling (FDM), fused filament fabrication (FFF), big area additive manufacturing (BAAM), robocasting, cellular fabrication (C-FAB), and variations on metal injection molding (MIM) or ceramic injection molding (CIM) fall into the material extrusion family. Future innovations in this family include further penetration into large scale applications and materials advances.

Figure 13: Cincinnati's BAAM had pushed the bounds of FDM scale and applicability.
Source: https://www.e-ci.com/baam

Figure 14: The BigDeltaWasp printer uses a mud-like feedstock.
Source: https://www.3dwasp.com/

Figure 15: ORNL and MVP partnered in the development of the RAM system, the world's first large scale thermoset printer.
Source: https://3dprinting.com/

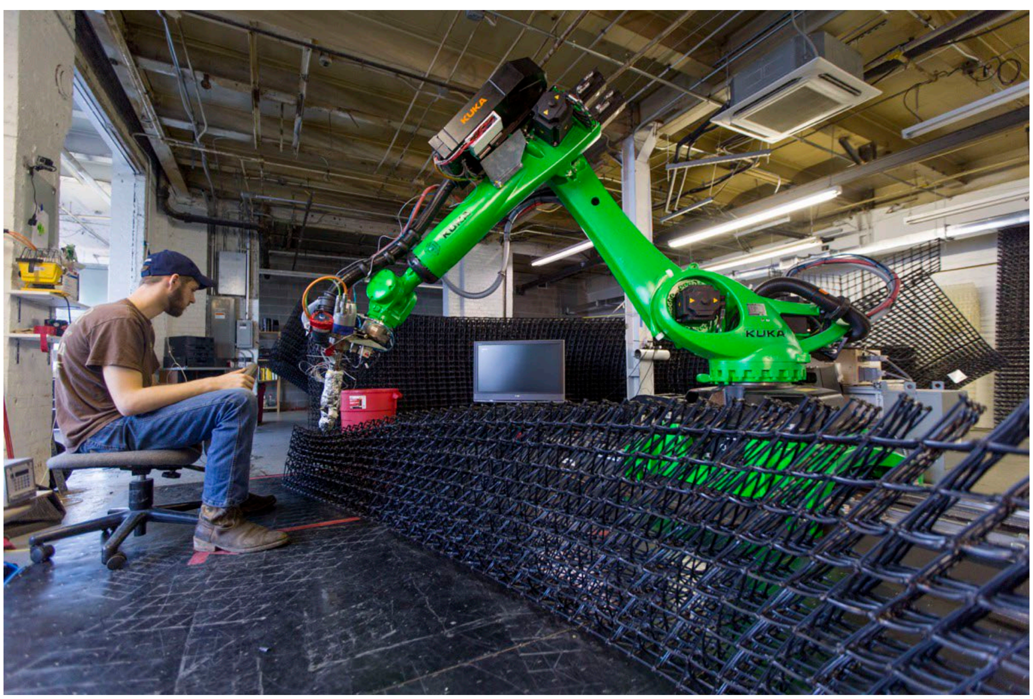

Figure 16: Branch Technology leads the charge in C-FAB development.
Source: https://www.3dprintingmedia.network/

2.7 SHEET LAMINATION

Sheet lamination is defined in ASTM 2792 [13] as “an additive manufacturing process in which sheets of material are bonded to form an object.” This process forms, stacks, and bonds thin sheets of material to construct an object. Bonding methods include adhesives, ultrasonic welding, brazing and thermal bonding. Forming methods include CNC milling, laser cutting, vinyl cutting, and aqua blasting. Build materials include paper, plastic, composites, and metals [27]. By nature, sheet lamination processes incorporate hybrid methodologies. Two categorical methodologies of the process are used, termed “cut then stack” and “stack then cut.” These two methodologies refer to the order of operations performed [51]. “Cut then stack” methods, in which sheets are literally cut and then stacked, result in overall material savings at the price of geometrical design freedom, while “stack then cut” methods, in which sheets are cut after they have been stacked, allow for greater geometrical design freedom at the cost of material usage. For “cut then stack” methods, the cut cross-sections must be stackable on top of each other [52]. Multi-material parts, as well as embedded sensors or components, are feasible. Sheet lamination enables large-scale parts and does not require support structures. However, layer height is limited to the thickness of each sheet, material removal can be time-consuming and wasteful, and bond strength is driven by the lamination technique used [46]. Fabrisonic’s UAM process builds metal components with a major advantage of no residual stress accumulation throughout the build process. Additionally, removing material from internal voids can prove problematic depending on the exact system configuration. Build volumes vary widely, depending on the material used. Larger build volumes, up to $4m^3$, are seen with composite and metal-based processes, while other materials range on the scale of $0.01m^3$. Processes such as ultrasonic additive manufacturing (UAM), laminated object manufacturing (LOM), selective lamination composite object manufacturing (SLCOM), plastic sheet lamination (PSL), computer-aided manufacturing of laminated engineering materials (CAM-LEM), and composite based additive manufacturing (CBAM) fall into the sheet lamination family. Future innovations in this family include large scale part production in UAM among others.

Figure 17: Impossible Objects' CBAM-2.
Source: https://www.impossible-objects.com/

Figure 18: Fabrisonic's SonicLayer 4000 utilizes the UAM process to produce parts.
Source: https://fabrisonic.com/fabrication/

3. DESIGN GUIDELINES FOR LARGE-SCALE ADDITIVE MANUFACTURING

Large scale AM is categorized by print volumes that are at least 15 times the build volume of desktop-size, consumer-level AM systems [53]. Not all families of AM are well-suited to manufacture components at this scale due to varying considerations, from mechanical machine framework to feedstock unit price, currently achievable process rate, or end part mechanical properties.

The mechanical machine framework can limit a process' adaptability to large-scale applications because, for many machines, the maximum build volume is encapsulated within, and therefore limited by, the machine volume itself. More flexible frameworks, like those that use robotic arms, can allow for a lower overall equipment cost for larger build volumes. However, not all processes are well-suited to such flexible frameworks. Material extrusion and directed energy deposition have been shown as the most well-suited to flexible frameworks.

The cost to produce an AM part encompasses many factors [54-56]: initial machine cost, feedstock material cost, machine time, supporting labor required, build volume utilization [57], and energy consumption, among others. In scaling up each family, these costs correspondingly increase. Two costs that have been consistently shown as the major contributors to part cost are the feedstock material cost and the initial machine cost [58]. At large scales, the feedstock material cost becomes increasingly important in the economic model. Where high material unit costs at a small scale may be justified thanks to geometric freedom and low production quantities, these trade-offs become exorbitant at large scale. Specifically, the unit price of the most common materials used in vat photopolymerization, material jetting, powder bed fusion, and metal binder jetting is no longer justifiable at large scales.

Initial machine cost can be much higher for some processes, such as powder bed fusion, due to requirements for environmental controls or key components of the system infrastructure. For example, in the case of PBF and some instances of DED, an inert or vacuum environment is required for many materials. Other processes may require specific ambient temperatures, pressures, or humidity levels for proper performance. Powder based processes often require special powder handling systems for loading, cleaning, or recycling powders. These types of requirements further limit the scalability for vat photopolymerization, powder bed fusion, material jetting, and some binder jetting processes.

Comparing the process rates for different AM processes can be complex due to the variety of operating principles. For example, the powder-based processes include two major stages at each layer: powder spreading and adhesion (i.e. melting, sintering, binding, etc). In contrast, material extrusion processes are largely continuous throughout a layer. In some cases, it makes sense to compare volume per hour (ME). In others, it makes more sense to compare weight per hour (DED), and for others still, it makes sense to compare layer cycle times (binder jetting). Regardless, for scalability, a process must be capable of generating large volumes in a short time to be feasible. For current incarnations of vat photopolymerization and powder bed fusion, this requirement is a major faltering point. However, concepts to increase their process rates by moving beyond single point processing (i.e. one laser spot exposing a path each layer) to multi-point processing (i.e. multiple laser points operating simultaneously in each layer), line-wise processing, or even layer wise processing (i.e. exposing the entire layer at one time using masks) may help overcome this barrier.

The mechanical properties produced by some AM families/materials at the small scale become nonsensical when considered for large-scale applications. For example, the photopolymers used in vat photopolymerization and material jetting typically do not perform as well as common engineering plastics and their performance degrades with UV exposure.

Table 1. Suitability of AM Families to large scale processes

Process	Suited for LSAM?	Why/why not?
Vat Photopolymerization (VP)	No	material unit cost, mechanical system feasibility with vat, part properties over time, low process rates
Powder Bed Fusion (PBF)	No	material unit cost, low process rates, environmental controls
Binder Jetting (BJ)	No	material unit cost, feasibility of powder bed and furnace sizes/times
	Yes	used at large scale with sand casting molds
Material Jetting (MJ)	No	unit cost of photopolymers, part properties over time
Sheet Lamination (SL)	Yes	used at large scale
Material Extrusion (ME)	No	unit cost of filament feedstock
	Yes	used at large scale with pellet feedstocks (unit cost) + screw extruder (processing rate)
Directed Energy Deposition (DED)	Yes	used at large scale (wire feedstock), limited by inert environment requirements

Vat photopolymerization, powder bed fusion, and material jetting are particularly well-suited for small-scale AM, while they face major limitations in their feasibility for large scale AM. On the other hand, material extrusion, directed energy deposition, sheet lamination, and 3DSP (binder jetting) have all been proven feasible at large scales; hybrid processes also play a critical role at this scale. Only these large-scale suitable families are addressed herein. Industry examples of large-scale application for each family are provided in Table 2.

Table 2. Examples of large-scale AM in industry, per AM family.

AM Family	Industry Example
Material Extrusion	BAAM, WinSun, AbisCor, Contour Crafting
Directed Energy Deposition	mBAAM, BeAM, EBAM, Arevo, WAAM
Binder Jetting	D-Shape, Viridis3D, Voxeljet, Desamanera
Sheet Lamination	Impossible Objects, SLCOM, Fabrisonic

Machine-specific information included herein draws from expertise on systems developed at the Manufacturing Demonstration Facility at Oak Ridge National Laboratory, as well as information available in literature in the public domain. Some processes and machines have been studied and published on more prolifically, while development on others is more nascent or lies outside the public domain at the time of writing this report. Opportunities for future research may include further development of systems well-suited for large scale additive manufacturing and their associated process or machine-specific parameters and limitations.

3.1 GENERAL DESIGN GUIDELINES

ISO/ASTM standard 52910 [13] highlights a critical general guideline: “if a part can be fabricated economically using a conventional manufacturing process, that part should probably not be produced using AM.” When designing for AM, it is critical that the unique advantages of AM are leveraged.

Figure 19 illustrates the complex considerations that are necessary when designing for AM. These considerations, as well as the design guidelines that are general to all large-scale processes, are discussed in more detail in the following sections.

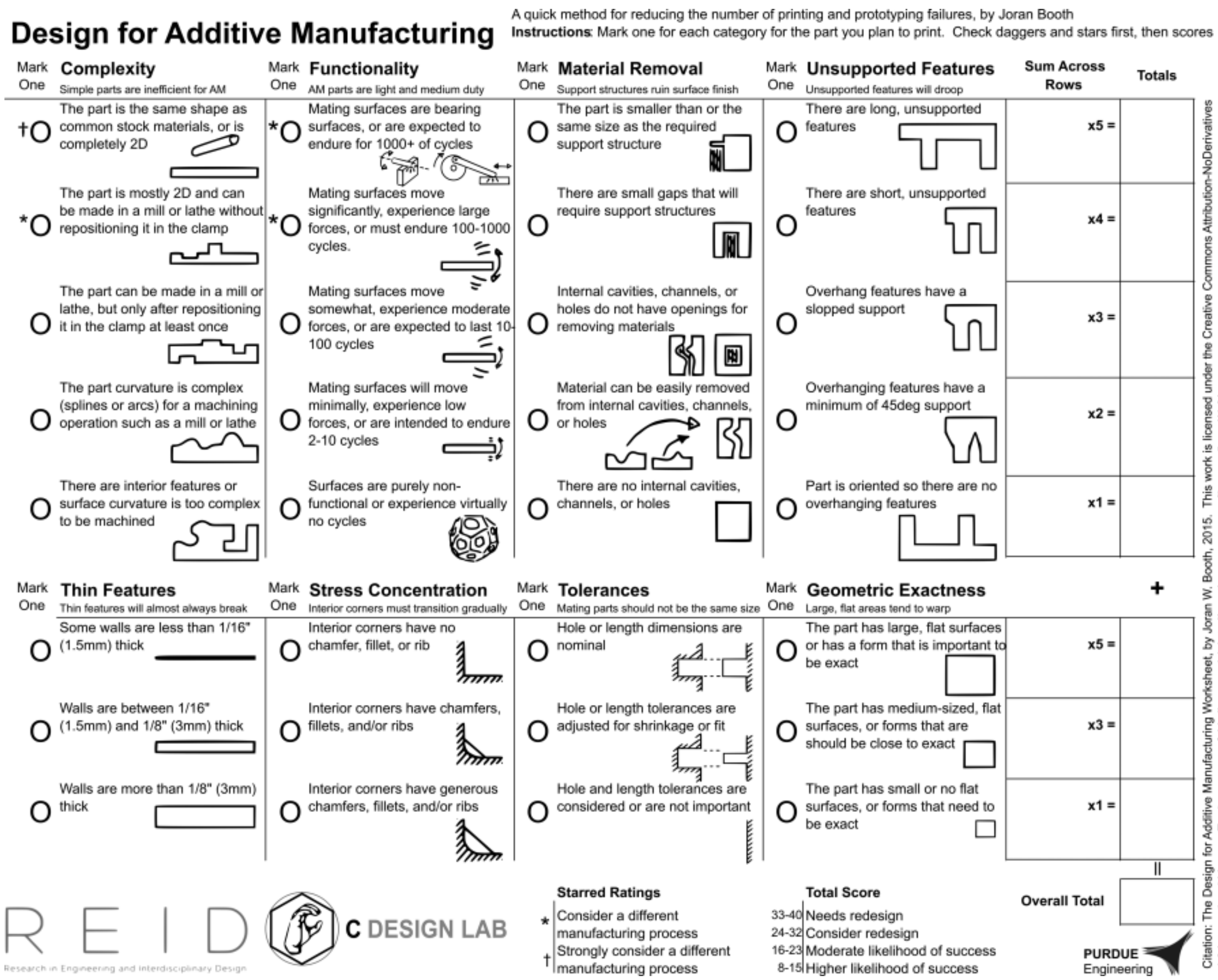

Figure 19. Considerations for designing for additive manufacturing, taken from [27]

3.1.1 Designing for End-Use: End Part Mechanical Properties

End part **mechanical properties** are highly sensitive to both process and material. Therefore, the AM process and material used for each part should be selected to meet the needs of the part's end use, and the part should be designed with the process and material in mind. Interlaminar bond quality draws attention in AM as common failure modes and **anisotropy** originate from inadequate bonding. When an end part will be subjected to mechanical loads, the lower expected strength in the vertical direction of the printed part must be considered in selecting print orientation. That said, methods to improve mechanical properties, such as heat treatment or adding tensioning rods, have proven effective.

3.1.2 Printable Geometries

Build orientation

One major consideration in AM is the **orientation of a part** within the build space. Because of the layer-based approach in these processes, the orientation of a desired geometry relative to these layers can affect directional strength and the surface finish of the end part, as well as the likelihood of success in the build. Considerations when choosing the part orientation include permissible overhang angle, residual thermal stresses induced, and part application or function. A part should be designed after the orientation has been selected, to prevent issues when pre-processing the design of the part, e.g. overhang angles and directional strength produce conflicting orientation requirements.

Overhang angles

The **overhang angle**, which can be material- and process-sensitive, refers to the most aggressive angle permissible before build quality suffers. It may be referred to as relative to vertical or horizontal, but the underlying concept is, particularly for ME and DED, that deposition over thin air without any underlying support structures is quite limited. On the BAAM system, the overhang angle limit is 45° from vertical [59], while the mBAAM system is limited to 15° from vertical [60]. Areas of a part where this constraint is not met are likely to exhibit poor build quality and may cause the build to fail. As such, holes and cavities are best oriented with their cross-section in the horizontal plane or should be eliminated from the print and then added in a post-process. Overhang angle considerations for binder jetting are most relevant when a sintering post-process will be performed. However, for 3DSP overhangs are not a major consideration in design. Overhangs in sheet lamination processes are more difficult to achieve in "cut then stack" approaches than in "stack then cut" approaches. Additionally, overhangs are rarely used in sheet lamination processes because, without underlying layers, the sheets often separate which produces poor mechanical properties.

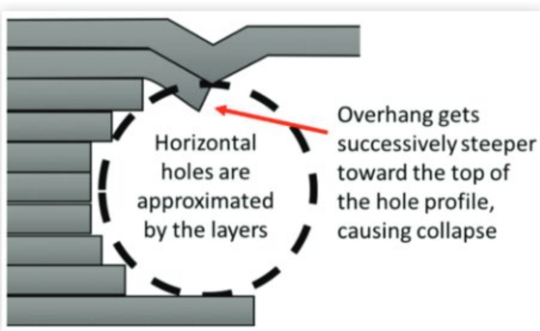

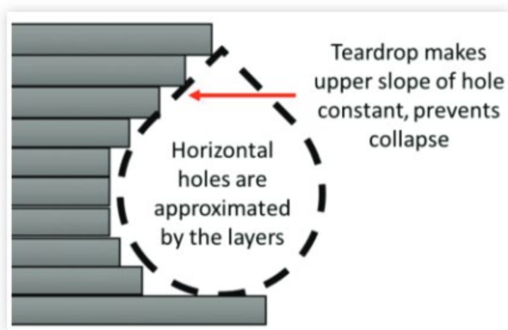

Figure 20. Left: A circular hole oriented horizontally (parallel to the layers of the build) will often collapse toward the top. Right: A teardrop-shaped hole can be oriented horizontally (parallel to the build layers) and is self-supporting. Taken from [27], Figures 4.12 and 4.13, respectively.

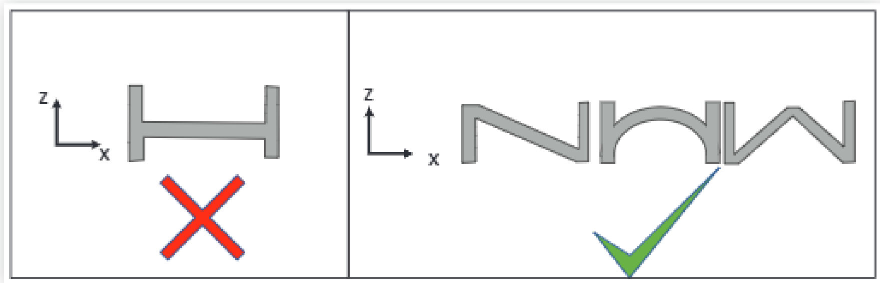

Figure 21. Avoid flat overhangs – use slanted, arched, or peaked overhangs. Taken from [27], Figure 4.23.

Bridging

Closely related to the overhang angle is the **bridging distance**. While an overhang can be described as a cantilever beam with only one end supported, bridging distance refers to a beam supported at both ends but unsupported in the middle. The maximum bridging distance is closely tied to the process material. Testing on BAAM indicated a maximum bridging distance between 1.85” and 2.25” for CF-ABS, depending on the nozzle [59]. Conservatively, bridging should be avoided, including in part cavities. Considerations for bridging in binder jetting are similar to those for overhangs, in that the sintering post-process presents the greatest risk for deformation. As 3DSP processes do not require sintering, bridging is not a major consideration in design. Cavities in both binder jetting and sheet lamination processes are possible as long as excess material removal is considered through the addition of outlet channels, escape holes, or machine tool access.

Support structures

Support structures are commonly used at smaller scales in ME processes to expand capabilities for overhanging and bridging geometry. However, at a larger scale the post-processing required to remove a support structure afterward is economically prohibitive [59]. Parts should be designed and oriented to be self-supporting—such that no support structure is necessary. For the BAAM system, parts requiring support structure can be subdivided into smaller portions that do not require support structure and bonded after printing. By nature, binder jetting includes support material throughout production.

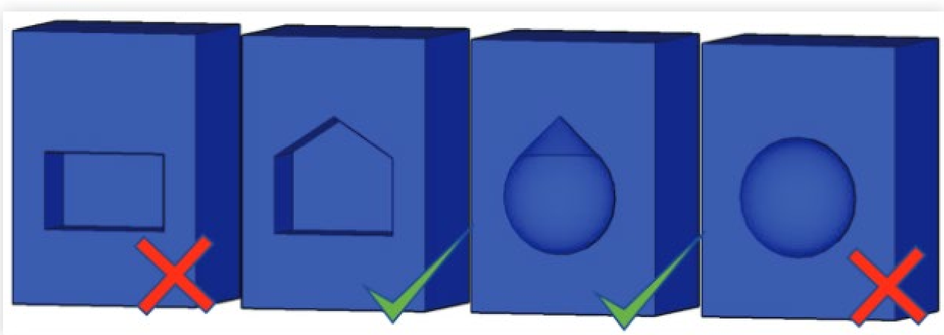

Figure 22. Cavities that are not self-supporting (far left and far right) and cavities in their modified version that are self-supporting (center). Taken from [27], Figure 5.11.

3.1.3 Special Cases, Work-arounds, and Up-and-coming Developments

Subject matter expert Michael Borish was consulted in writing this section.

Variations on and deviations from the standard orthogonal, layer-wise printing strategy are under continual development, as applications are limited by this standard method. Other methods that will be described here include: spiralization, continuous printing, non-planar surface contouring, and lattice filling. Each brings advantages for specific applications.

Figure 23: Two methods of slicing were used to create the same geometry. Note the stair-stepping artefacts on the right are less prominent on the left. Taken from [61].

Spiralization refers to a method of combining the normally discrete, or separate, layers of a print [62]. This is done by setting a single point as the start and stop positions of each layer, i.e., each layer has the same starting point and the same stopping point, and the two points overlap. Then, transitioning from one layer to the next is smooth, rather than separated by a start and stop at each layer. Thus, in the case of a cylinder, one could envision this technique as the difference between stacking discrete rings vs. forming a tight helix. This technique is currently not well-suited for geometries with infill patterns or other open (not closed loop) paths. Because there are no stops and starts, the build is less prone to defects at start/stop conditions, and the build time decreases.

Continuous printing is related to spiralization, although continuous printing encompasses a broader scope of techniques. One method of continuous printing is known as 45-degree printing, wherein the build platform is, for example, a conveyer belt (see PowerBelt3D or BlackBelt for ME example). Alternatively, the use of tilt and turn tables in DED processes allows for radially continuous printing, where the concept of a layer in the conventional cartesian sense begins to fade (see Figure 9). The use of additional axes of motion outside the typical 3 also allows for multi-plane printing [63]. Oftentimes in continuous printing the build platform is angled, rotated, or moves in such a way that allows the printhead to continuously print. In other words, the printhead does not need to perform any stops or starts because the part being printed is moving around, allowing material to be deposited in the necessary places.

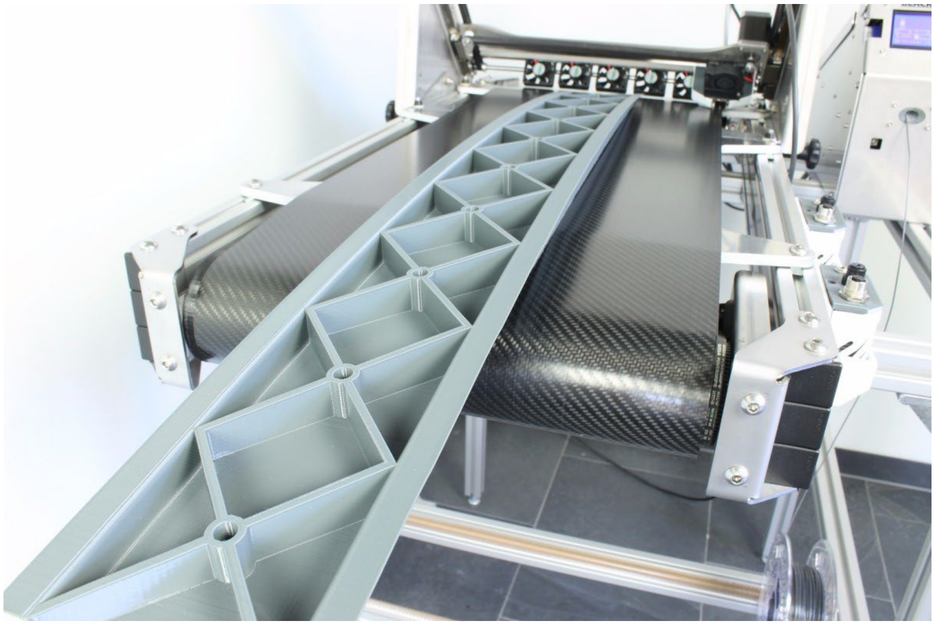

Figure 24: An example of a conveyor belt printer, the BlackBelt.
Source: https://newatlas.com/blackbelt-3d-printer-conveyor-belt/49864/

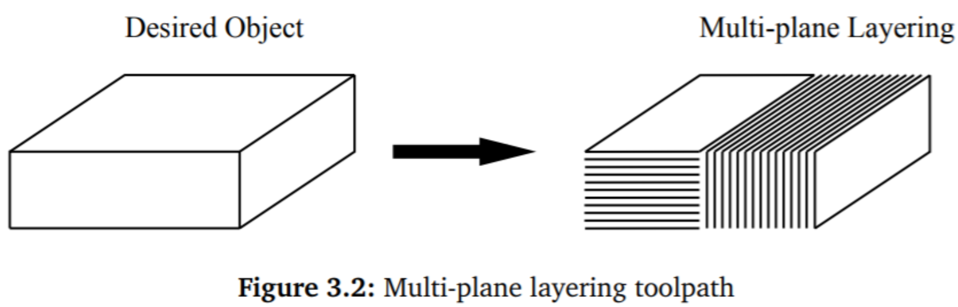

Figure 25: A graphic depicting the multi-plane layering concept. Taken from [63].

Non-planar surface contouring is another alternative approach that is currently under development. The standard orthogonal printing strategy is based on a perfectly flat, planar surface as the starting surface from which to print. In non-planar surface contouring, this starting surface is not planar. Convex, concave, and complex curvatures may be approached, with varying limitations to each. Kinematic arrangements with greater than 3 degrees of freedom may be required for successful implementation [64]. In general, these techniques are limited to gentle curvatures, because steep curves and/or corners pose challenging computational problems [65].

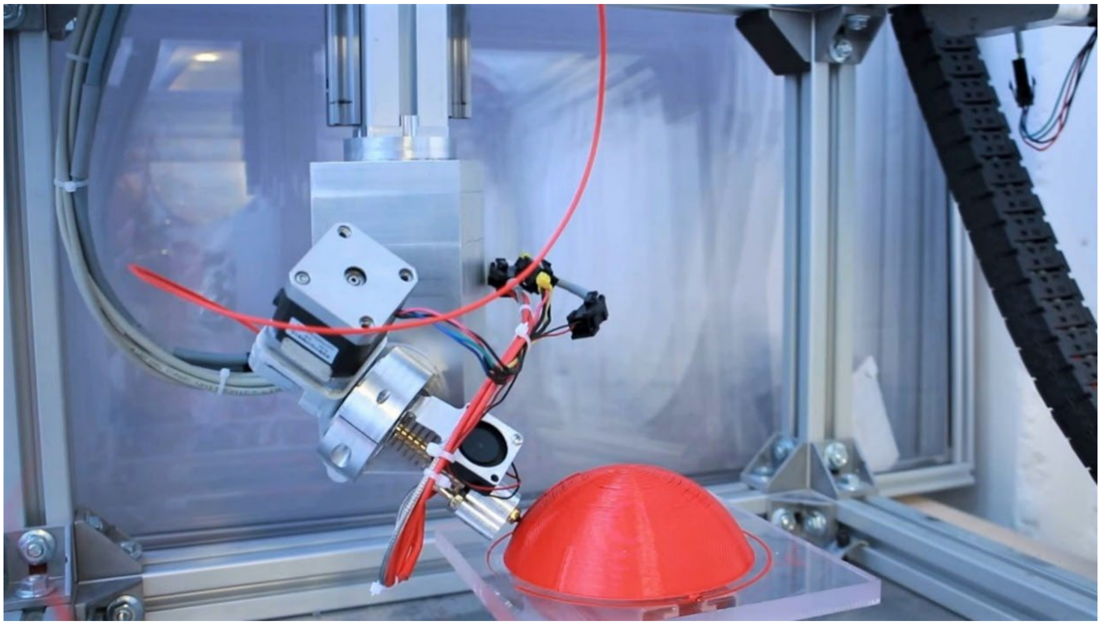

Figure 26: A 5axismaker prints a nonplanar surface contour.
Source: https://all3dp.com/2/5-axis-3d-printer-the-latest-advancements/

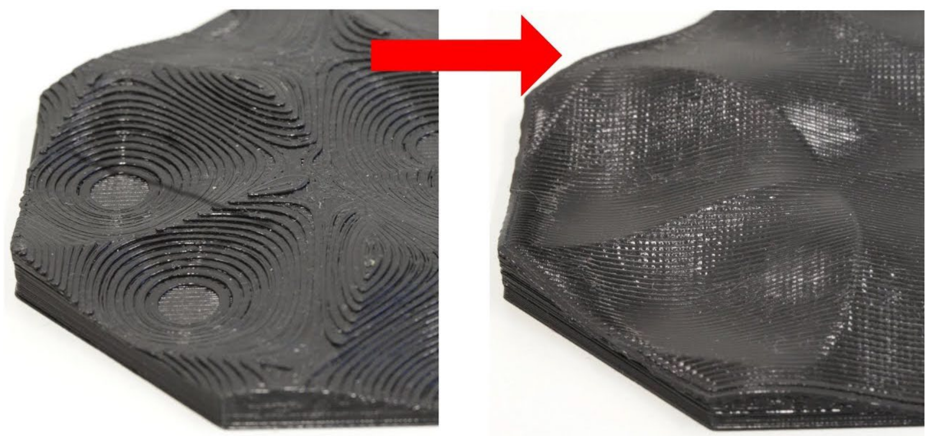

Figure 27: Non-planar surface contouring can greatly improve the surface roughness by avoiding the stairstepping defect. Taken from [65] and https://www.youtube.com/watch?v=km1lvuva5mI

Lattice filling encompasses approaches that do not yield a fully dense structure. Many variations of lattice geometry exist, and their design can be tailored to enhance light-weighting, impact resistance, strength, or other structural characteristics. The use of various lattice structures and scales can yield lightweight structures with impressive mechanical properties and performance. Significant work has been pursued particularly with material extrusion of carbon fiber-filled polymer materials, as fibers preferentially align with the extrusion direction. This technique has been termed wire frame printing [63] and can yield unique possibilities for enhancing mechanical performance. Lattice structures for powder-based processes are more easily achieved due to the inherent support structure of the surrounding powder. One industry example of implementing lattice filling is Branch Technologies.

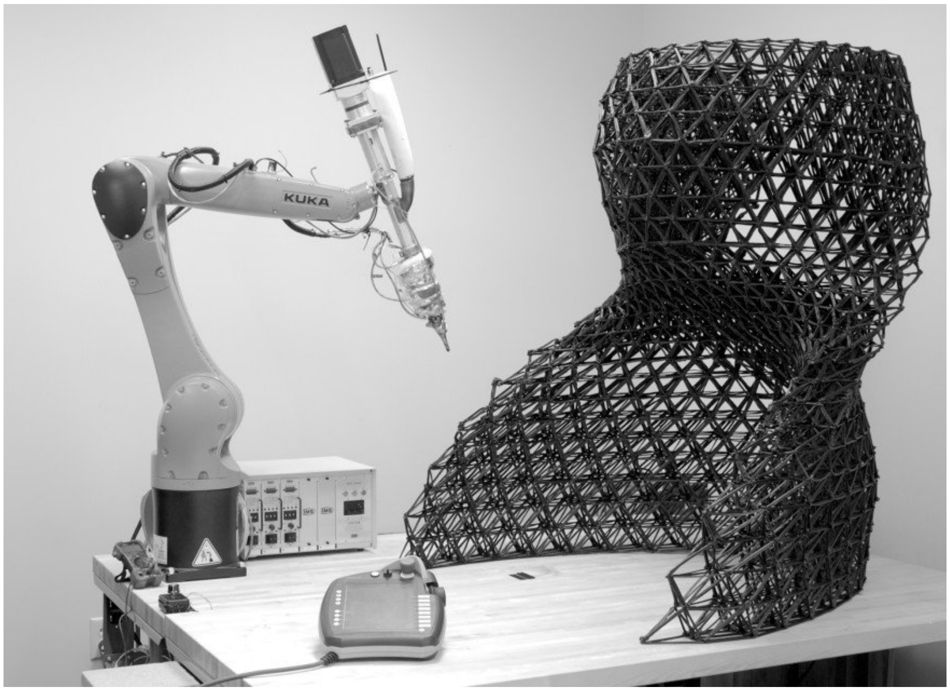

Figure 28: Wire frame printing can quickly fill volumes with unique mechanical and structural properties. Source: https://3dprinting.com/tips-tricks/3d-printed-lattice-structures/

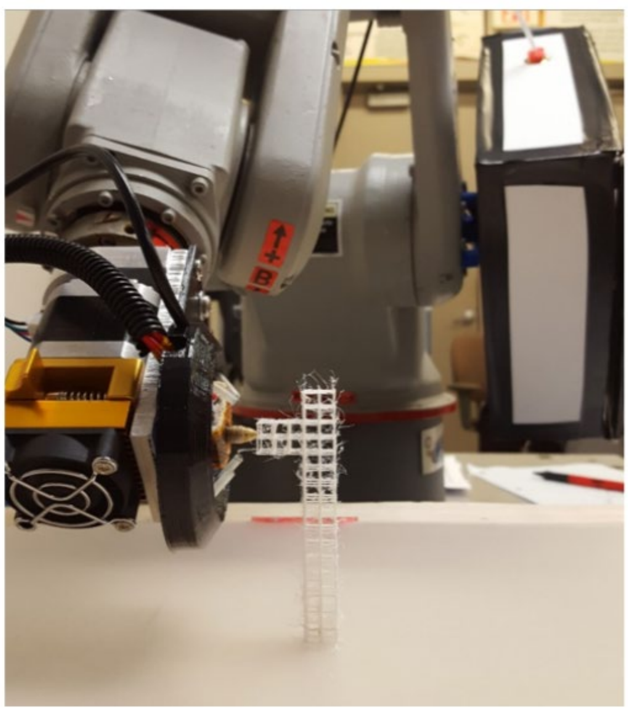

Figure 5.3: 3D lattice structure printing process

Figure 29: Lattice printing can be achieved through various slicing and process execution strategies. Taken from [63], figure 5.3.

3.2 GENERAL PROCESS PARAMETERS & POST-PROCESSING

3.2.1 Build rate & bead geometry

The **build rate** and **bead geometry** are inherently related and are particularly important in large-scale additive ME and DED processes [66]. Large-scale processes prioritize high deposition rates, often at the price of small features. Bead geometry describes the size and shape of an individual bead, where a layer is constructed of beads. As bead geometry becomes smaller, finer feature details can be resolved in a part. However, these details come at the price of production time. On the BAAM system, bead geometry is tied to the nozzle size, but is typically 10mm wide by 4mm tall [59]. The typical build rate is between 50 and 65 lb/hr, with a theoretical maximum of 100 lb/hr [59, 67]. The mBAAM system has a bead height of about 2.3mm, with two parallel beads resulting in a wall approximately 12mm wide [68]. 3DSP binder jetting processes can reach print speeds of 135 L/hr with submillimeter layer heights. Sheet lamination layer heights are limited to the thickness of the sheets used, as are build rates.

3.2.2 Layer time, bonding & residual stress

Thermal AM processes introduce **residual thermal stresses** into the part with cyclic thermal cycles. As a consequence, part **warping** or layer **delamination** may result from oversights in process planning. To evade these defects, the time spent on each layer (**layer time**) must be such that a prior layer is neither too cool nor too hot. Proper layer bonds are formed above a minimum temperature while structural integrity can be maintained below the melt temperature. These temperature bounds and the cooling rate are sensitive to the material used, the geometry under construction, and the ambient conditions of the print. Geometries with a larger surface area to volume ratio will have a shorter layer time, while those with a smaller surface area to volume ratio will have a longer layer time. Best results on the mBAAM system are achieved when the layer time is minimized [60]. One major advantage to binder jetting processes is the lack of residual thermal stresses, as these processes occur at or near to room temperature, so no large cyclic thermal gradients are induced during part production.

3.2.3 Post-processing

Post-processing refers to all steps taken after the additive process is complete before the end part can be used. Machining, polishing, or heat treatment are all examples of potential post-processes. It is recommended to design with post-processing in mind, whether that be tool accessibility for machining or overbuilding the part to near net shape such that high tolerance mating surfaces can be achieved. Large scale processes typically target a near-net geometry and require post processing for surface finish, tolerancing, or feature addition (holes).

3.3 MACHINE-SPECIFIC LIMITATIONS

3.3.1 Material Extrusion: BAAM

General Guidelines

Subject matter experts including Alex Roschli, Celeste Atkins, and Phillip Chesser were consulted in writing this section.

There are many general design rules for BAAM, as well as material-specific considerations. Here, general guidelines for achieving desired dimensions, successfully printing a geometry, and achieving the desired mechanical performance are discussed. These guidelines apply generally unless a material-specific guideline dictates otherwise.

Achieving Desired Dimensions: Bead Geometry, Resolution, and Post-Processing

In general, there are 4 options for nozzle size with 4 corresponding bead widths, as shown in Table 3 [59]. The most used nozzle is the 0.3" and the least used nozzle is the 0.1". As such, system tuning and overall part quality with the 0.3" nozzle exceeds that of the 0.1" nozzle. The greater back pressure in the extruder when using the 0.1" or 0.2" nozzles results in more accentuated transients and oozing at lifts and travel movements. Smaller nozzle sizes also require lower layer times, as the change in surface area to volume ratio of the resultant bead causes higher solidification rates. These combined considerations limit the print speeds and the scale of feasible and printable objects when using 0.1" or 0.2" nozzles. The general rule of thumb for minimum layer time used as a starting point for material and geometry calibration is shown in Table 3. When critical surfaces of the part will be machined in their post-processing, the 0.4" nozzle is used. The layer height is regarded as ½ of the nozzle diameter, as shown in Table 3.

Table 3. Common nozzle diameters and their associated bead widths, heights, and minimum layer times

Nozzle Diameter (in)	Bead Width (in)	Bead Height (in)	Min Layer Time (sec)
0.1	0.11	0.05	60
0.2	0.22	0.1	75
0.3	0.34	0.15	90
0.4	0.5	0.2	120

* Taken from [59], Table 3. Minimum layer time column added.

Bead geometry must be considered when designing, as features with dimensions of non-integer multiples of bead width will not print as desired [11]. Wall thicknesses should thus be designed as even multiples of bead width (typically 2, 4, or 6). Odd multiples are permissible but will result in a less efficient printing process due to added starts, stops, lifts, and travels; as such, unintended voids or other defects may occur [69]. One bead of material cannot be accurately placed in an area that is much less than or much greater than a bead width. Attempts to do so will either result in overfilling or voids, respectively.

Two less-intuitive examples where bead geometry matters are holes and corners [11, 48]. When printing holes whose axis is perpendicular to the XY plane, if hole spacing is too small, unintended voids in the spaces between them may result. As such, post-processing to add in holes after printing may be a better alternative. When sharp external corners are required and machining as post-processing is anticipated, overbuilding at that corner edge is needed, as shown in Figure 30 [70-72].

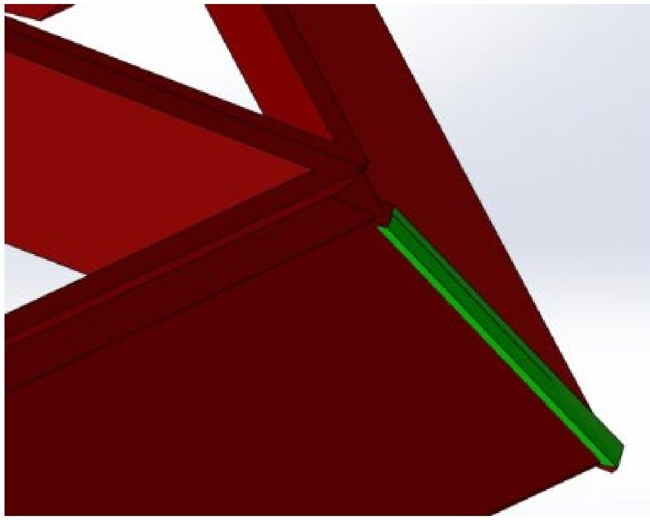

Figure 30. Green section representing an extended corner. Taken from [70], Figure 6.

In general, machining as post-processing is leveraged to achieve features whose size is near to or less than that of half of the bead width. Even with machining, tolerances tighter than 10 thousandths of an inch are nearly impossible. Resolution or accuracy on a local scale is largely a function of bead geometry. However, on a global (whole part) scale, factors including the feedstock material properties, the part geometry, and the thermal cycles contribute to generation of residual stresses and warping. Attempts to print large, thin, flat sheets are often thwarted by residual stress-induced warping.

When machining is anticipated, the part will be printed to “near net shape”. This means that it will be overbuilt by just enough so that after machining the desired dimensions, tolerances, and finish will be achieved. Specifically, surfaces where machining will occur are thickened or offset outward by ½ of a bead width in the printed XY plane or ½ of a bead height in the printed Z direction. This is done so that the machining process will remove ½ of a bead and the resulting surface will be free of voids and defects. However, this rule of thumb must be adjusted for special cases, including holes, corners, and very large and flat faces. The ORNL Slicer has a feature to adjust all surfaces outward, but this may lead to issues with internal geometries or holes and should be used with discretion.

The best surface finish achieved to date with a printed part is an automotive standard Class A finish [73]. This required extensive post-processing, from machining to sanding to polishing and coating. For as-printed parts, the surface finish within a layer is better than that of surfaces that span many layers. For example, the max deviation of a part printed from CF-ABS with a 0.3” nozzle was measured in-plane and layer to layer: 0.059” and 0.18”, respectively [59]. It should be noted that these values are dependent on the nozzle size (bead geometry) and the material.

Printability: Bridging, Infill, and Overhangs

Bridging capabilities on BAAM are influenced by material, environmental conditions, and nozzle size. For CF-ABS, the maximum bridging distance with a 0.3” nozzle was measured to be 1.85”, while a 0.2” nozzle yielded 2.25” [59]. When bridging is required for a feature, a 45-degree support can be added beneath it to decrease the bridging distance required.

The term infill arises mainly in the slicing process as a clear distinguishment between path types [11]. There are about seven different path types. The main purpose of infill is to fill a part and provide structure with minimal time and weight. Using infill on BAAM parts is not a common practice, but when used the standard density is 50%. Due to poor bridging capabilities at this scale, it is not advisable to design for infill density less than 25%. Typical infill patterns used include grid, hex, and concentric. Infill is related to bridging because infill will need to be spanned by skins to create an acceptable top surface. Typically, three layers of skins are applied to achieve a strong and flat top surface that doesn't show sagging between infill supports. When machining is anticipated, more skins (6) are applied to maintain part strength during and after machining.

The rule of thumb for overhanging geometries on BAAM is 45 degrees from the vertical for non-compounded angles [59]. However, compounded angles can allow for steeper angles (up to 70 degrees from the vertical) or shallower angles, depending on whether the compounding is convex or concave, and its severity. Layer time and part geometry also play an important role in achievable overhangs: shorter layer times allow for more aggressive overhangs because a warmer polymer better bonds to itself. That said, if the layer time is too short, sagging will occur, as opposed to failure by the bead essentially rolling off. The steepest overhangs, up to 70 degrees, are achieved for geometries similar to a traffic cone, where the part is pulled to support itself as deposited material cools and solidifies. Regardless, it is strongly advised to stick to the rule of thumb in most cases.

Achieving Desired Performance: Mechanical Properties

Mechanical properties for BAAM printed parts are largely material- and geometry-dependent. Using ABS material on the BAAM system, end parts exhibit near-isotropy with excellent interlaminar adhesion. However, a change in material to CF-ABS results in more pronounced anisotropic properties [59]. Some level of anisotropy in the printed Z direction is consistently seen throughout all layer-based additive processes. For example, in the X-direction, the average UTS and elastic modulus of a CF-ABS printed part on BAAM was found to be 11-12 ksi and 1.6-1.8 Msi, respectively. In the Z-direction, the average UTS and elastic modulus were 2-3 ksi and 0.35 Msi, respectively [74]. This anisotropy must be considered in the design of load-bearing structures.

A few printing methods to enhance part strength and performance include randomizing starts and stops, zippering, z-pinning [75], and post-tensioning [72, 76]. "Starts and stops" refers to the points along the path in a layer where printing will begin and subsequently end. When the same place is selected for all layers, a seam will be visually evident; this is a place where stress concentrations or defects may arise and lead to premature part failure [62]. Changing where the start and stop points are, from layer to layer, prevents the stress concentrations from stacking up and enhances end part strength and performance. Zippering is another method to evade stress concentration at seams. However, these seams are due to pathing artefacts rather than starts and stops. In this situation, the location of the seam is moved by 2-3" in alternating layers, creating a pattern from layer to layer similar to that of a zipper.

In Z-pinning, holes in the Z-direction are left during the beginning of the printing process [75]. Later in the printing process, these holes are filled all at once. This method provides an interlaminar bond far superior to the interlaminar bonds of the standard printing techniques. Testing with CF-ABS on BAAM showed a "9.75% increase [in tensile strength in the Z-direction] in comparison to a part with solid infill and a 51% increase [in tensile strength in the Z-direction] in comparison to a part with 75% dense infill" [49, 75].

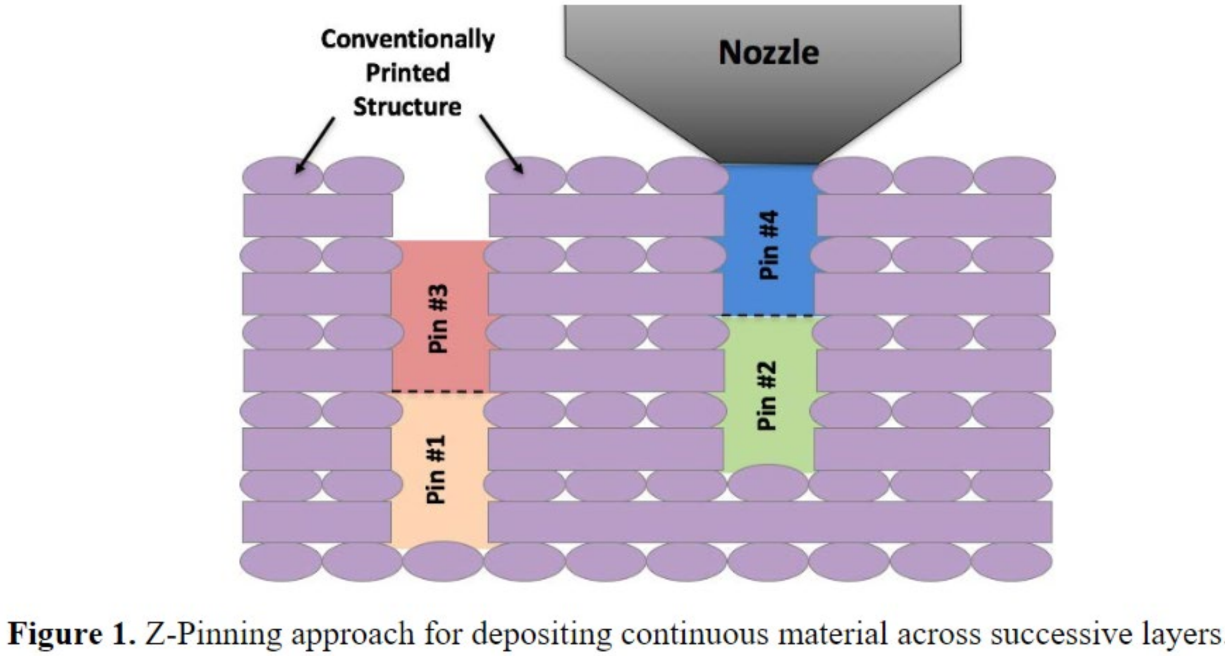

Figure 31: From [75], figure 1. "Z-pinning approach for depositing continuous material across successive layers."

Post-tensioning methods to improve the performance of load bearing structures have been tested and proven with BAAM as well. The employed methods are similar to those used in post-tensioned concrete structures. These methods can allow the designer to ensure compressive stresses are only found at layer boundaries, where typical tension failure modes, such as delamination, originate. To design with post-tensioning in mind, one must clearly understand the loads on the structure and its stiffness. Post-tensioning tendons can be selected and placed strategically, such that their relative stiffness is at least 10x lower than the structure and the post-tensioning force is uniformly applied across the structure's cross-section [72, 76].

Material-specific Guidelines

Subject matter experts were consulted for different materials: Vidya Kishore and Tyler Smith for foams and Halil Tekinalp for biocomposites.

Material-specific considerations when designing for BAAM include mechanical performance, thermal performance, layer time considerations, and process rates. The base materials used on BAAM are engineering thermoplastics, both semicrystalline and amorphous, including: ABS, PLA, TPU, and PS. Materials with higher compression ratios, such as PPSU, PPS, or PSU have maximum throughput rates near 40-50 lbs/hr. Variations on these base materials through fiber-filling or foaming are used to enhance the material properties for a particular application. Fiber-fill materials include: glass fiber (GF), carbon fiber (CF), and natural fibers like bamboo, pine [77], and poplar fiber or wood flour. Fiber fills are used to improve the base material's mechanical properties, such as tensile strength and stiffness, as well as decrease the material's coefficient of thermal expansion. Fiber reinforcement is determined by fiber dispersion, aspect ratio and interfacial adhesion between filler and matrix [78]. However, these benefits come at a trade-off with material density: the greater the fiber fill, the greater the density.

Foaming is used to decrease the material density, which is helpful for light weighting applications [79, 80]. There are two main methods to foam a base material for BAAM: using hollow glass microspheres

(HGMs) or using expandable microsphere foams. However, the tradeoffs here include high sensitivity to process parameters and potential decreases in material properties when compared to the base material. The materials discussed in this document will include neat ABS, 20 wt% CF-ABS, GF-ABS, expandable microspheres foams, syntactics foams, and PLA with natural fibers. Further details on these materials and more are available in the materials document package and in referenced publications.

Fiber-fills

One advantage of fiber-filled ABS materials is a marked reduction in residual stress warping as compared to neat ABS. This is because the CTE of the CF-ABS material is anisotropic: it is greater in the Z direction than XY as there is no fiber alignment in the Z direction. Fiber-filled materials also result in heavier and stiffer parts. Parts from recycled CF-ABS materials have increased Z-strength when compared to the virgin CF-ABS parts. The differing thermal behaviors of these materials corresponds to differing layer time considerations. That is, minimum and maximum layer times for neat ABS are about 2 minutes and 5-6 minutes respectively, while for fiber-filled ABS these are 90 seconds and about 10 minutes respectively. Typical throughput rates for neat ABS are comparable to CF-ABS, but about 5% lower. However, with fiber-filled ABS the maximum throughput is inversely proportional to the fiber-filling ratio. In other words, 40%wt GF-ABS maxes out at about 60 lbs/hr while 20%wt CF-ABS maxes out at about 100 lbs/hr. However, when averaged across the entirety of a part, the throughput rate with CF-ABS is about 60 lbs/hr thanks to non-printing moves. However, using a 0.1” nozzle restricts the throughput rate to about 15 lbs/hr because of gantry speed limitations. It should be noted, therefore, that reducing the number and length of non-printing moves effectively increases the overall throughput rate of printing a part.

Foamed Materials

HGM foams, also known as syntactics, are blended into the feedstock pellets by the manufacturer. The typical CF-ABS material prints well and results in densities in the range of 0.7-0.9g/cc. Bead geometry follows the same correlation as given in Table 3. Common nozzle diameters and their associated bead widths, heights, and minimum layer timesfor the most part. Bridging and overhang design considerations also follow the general guidelines for BAAM. Minimum layer times with syntactics are slightly less than their non-foamed counterparts, but higher than those foamed with expandable microspheres, due to the changes in thermal mass. However, the differences are small enough that the 90 second minimum is still used. Layer times of 15 minutes or more have resulted in excessive warping and led to part failure as well.

Expandable microspheres are purchased as separate pellet beads which are blended in a gravimetric blender with the base material pellets. The pellets themselves are a hydrocarbon blend which expands at elevated temperatures, in this case while inside the extruder. These are used with low-temperature polymers, including ABS, PLA, PS, CF-ABS, GF-ABS, PETG, and various biomaterials. Densities as low as 0.25g/cc have been achieved with many of these materials, using up to 10% foaming agent content. Depending on the processing parameters (extrusion rate, processing temperature, nozzle size, etc) and foaming agent content, extrudate will exhibit cross-sectional expansion upon exiting the nozzle, similar to die-swelling. This can result in a bead width up to twice the nozzle diameter in expandable microsphere foams. By strategically selecting the processing parameters and foaming agent content, bead widths from 0.13” to 0.8” and corresponding heights from 0.1” to 0.5”, respectively, can be achieved. However, it should be noted that as the foaming agent content increases, the tradeoff is in the mechanical properties and performance. It should also be noted that as the extrusion rate increases, the density of the extrudate decreases, thereby similarly diminishing mechanical properties.

Overall, printing with expandable microspheres foamed materials is done at a slower extrusion rate than their non-foamed counterparts, due to lower melt strength. However, there is a more stringent lower bound to the throughput rate when compared to non-foamed materials. That is: when the extrusion rate is too low, the residence time of the material in the extruder results in material degradation. The upper bound to the extrusion rate is characterized by extrudate similar to confetti, as the material density has decreased beyond what is desired. Layer times vary per base material but generally are lower than their non-foamed counterparts. Special design considerations for expandable microsphere foams include a less severe overhang angle constraint of 30 degrees, thanks to their diminished melt strength and mass. When designing for a desired density, it is best to allow bead width and/or wall thicknesses to vary slightly according to the foam, as the amount of expansion is closely tied to process parameters.

Biocomposites

Biocomposites comprise another important category of feedstock materials for BAAM. These feedstock materials are composed of bio-based thermoplastic polymer and bio-based fibers. Because these materials are renewable, carry lower embodied energy, lower carbon footprint and have lower cost, they are considered favorable over other petroleum-based synthetic polymer-based feedstocks. The most common matrix/base material used in these biocomposites in this category is PLA due to its commodity price, commercial availability, and biodegradability. Some of the other thermoplastic base materials that can be used as a biocomposite feedstock in BAAM systems include polybutylene succinate (PBS), cellulose acetate, bio-based nylon (nylon 11) and PET. There are many different types of bio-based fibers [81] from nano- to mm-scale that can be used in these biocomposites including: wood flour, pulp fibers, cellulose nanofibrils (CNFs), cellulose nanocrystals (CNC), lignocellulosic compounds, and natural fibers such as bamboo, poplar, switchgrass, hemp and kenaf. While both the matrix material and the fibers are preferred to be bio-based, in some cases combination of bio-based and synthetic materials can also be used as a BAAM feedstock under this category.

The main design considerations for these materials as a BAAM feedstock are their rheology, material properties and the optimization of printing conditions. Use of different type of bio-based fibers may result in printed parts with varying mechanical properties. The filler composition, size, and shape impact the dispersion of the fibers and the interface between the fibers and the matrix material. Poor dispersion and poor interfacial adhesion can cause early mechanical failure and lead to low mechanical properties. Methods to treat the fillers prior to compounding by leveraging chemical surface treatments such as epoxy have yielded significant improvement in interfacial bonding and thus mechanical properties. Figure 32 and Figure 33 compile mechanical properties achieved with these types of biomaterials. In terms of printing, PLA-based materials have relatively longer layer times compared to commonly used BAAM feedstock CF-ABS, because these materials retain heat longer and have a lower glass transition temperature. The minimum layer time required is dependent on part geometry. For example, while 2.5 min layer time is sufficient for a two-bead wall part, in which the relatively high outer surface area/volume accommodates cooling, a thick solid block could require 4 mins or more with restricted convective cooling.

Table 2. Wood-based, including wood flours, sawdust, and barks, and lignocellulosic fillers used in materials extrusion AM processing. All samples were printed flat on the print bed with a default (±45) infill pattern unless otherwise noted.

Filler Component	Particle Mesh Size	Particle Size (Microns)	Polymer	Loading Level (wt.%)	Additives/Filler Treatment	Printing Temperature (°C)	Nozzle Opening (mm)	Layer Thickness (mm)	Infill (Amount, Pattern)	Mechanical Testing [f]	Ref.
Osage Orange (*Maclura pomifera*) Paulownia (*Paulownia tomentosa*)	230	≤63	PLA	12.5	Dried distillers′ grain [a]	220	0.4	0.34	100%	T	[19]
Beech (*Fagus sylvatica*)	~60	≤237	PLA	0–50	Milled	230	0.4	0.19	100% (Square)	R, FT	[38]
			PVAc/UF (adhesives)	7–87.5	Milled		3	2	85%	B	[29]
European Softwood	~200	75 (median)	UF	13	Hardener 2545 [d]	21	1.6	2		T, F	[30]
Aspen (*Populus sp*)	100	150	TPU	0–40	PEG 6000, chitosan and MDI[e]	185				T, R	[39]
Cork (*Quercus suber L.*)		27–733	PLA	0–50	Tributyl citrate	230	0.8	0.4	100%	T, I, DMA	[40]
MDF Furniture Waste	~200	80	PLA	10 to 40 (vol. frac.)	Milled	185	0.5	0.15	25–100%		[37]
Microcrystalline cellulose (MCC)			PP/PE	0–10	Silane[g]	190	1.75	0.2	100%	FT, DMA	[41] [h]
			PLA	1,3,5	Titanate	165–190		1.55[i]	60%	FT, DMA	[20] [h]
Cellulose Nanocrystals (CNC)			BTPE[j]	0–60	Polymer-grafted	178	0.4	0.42	20%,100%	T, R	[42]
			PVOH	0–10	MCC acid hydrolysis	230	0.35	0.2	100%	T, DMA	[43]
Cellulose Nanofibrils (CNF)			PLA	0–30		180–215	0.4	0.2	100%	T, DMA	[44]
			PHB	0–3		75			100%	T	[45]
			PLA	0–5	Grafted with PLA	165	1.75			FT	[46] [k]
Pine Kraft Lignin			PLA	0–15		205	0.2–0.4	0.1	100% rectilinear	T, FT	[15]
Softwood Lignin			PLA	0–40		205–230	0.4		100%	T	[47]
Organosolv Lignin			Nylon 12	20–40	Carbon fiber added	210	0.5	2.5	100%	T, R, DMA	[24]
Organosolv Lignin Softwood Kraft			ABS, HIPS, Nylon 12	40–60	Carbon fiber added	210	0.5	2.5	100%	T, R, DMA	[23]

[a] Used to extract residual oils using hexane. [b] Used wood pulp. [c] Used wood flour. [d] Commercial hardener for UF (Glues Direct, UK). [e] PEG 6000: polyethylene glycol 6000, MDI: diphenyl methylpropane diisocyanate. [f] Tensile (T), rheology (R), bending (B), flexural (F), dynamic mechanical analysis (DMA), filament tensile testing (FT), impact (I). [g] Contained compatibilizer SCONA TPPP 9212 GA (0.6 wt.%, BYK-Chemie GmbH, Germany), based on PP functionalized with maleic anhydride, and the processing stabilizer Add-Vance TH 130 (1.7 wt.%, Addcomp Holland BV, Netherlands). [h] Printed filaments and 3D prototype part. [i] Thickness of the final printed filament. [j] BTPE: bioplastic thermoplastic elastomer comprised of 2,5-furandicarboxylate, 1,4-cyclohexanedimethanol, and poly (tetra methylene ether) glycol. [k] Only filaments were tested, no 3D-printed prototypes were tested.

Figure 32: Table taken from [44], table 2.

Table 3. Mechanical properties of wood and lignocellulosic filled poly(lactic acid) composites collected using tensile testing data from selected references.

Polymer	Filler	Filler Amount (%)	Tensile Strength (MPa)	Elongation at Break (%)	Young's Modulus (GPa)	Ref.
PLA	Beech (*Fagus sylvatica*)	0	55 ± 4.3		3.27 ± 0.38	[38]
		10	57 ± 1.1		3.63 ± 0.5	
		20	49 ± 3.3		3.94 ± 0.24	
		30	48 ± 5		3.84 ± 0.55	
		40	42 ± 4.3		3.86 ± 0.54	
		50	30 ± 4.4		3.00 ± 0.56	
	Cork (*Quercus suber* L.)	0	60.03 ± 2.34	1.5 ± 0.01	3.344 ± 0.0967	[40]
		5	38.3 ± 0.6	0.8 ± 0.2	2.815 ± 0.127	
		10	26.1 ± 0.5	0.8 ± 0.2	2.111 ± 0.173	
		15	21.9 ± 1.4	0.6 ± 0.2	1.701 ± 0.167	
		20	19.4 ± 2.7	0.8 ± 0.2	1.455 ± 0.0731	
		25	17.2 ± 3.5	0.6 ± 0.2	1.375 ± 0.199	
		30	15.5 ± 2.5	0.6 ± 0	1.179 ± 0.234	
		50	10.4 ± 1.0	0.2 ± 0	0.985 ± 0.0743	
	Cellulose	0	53.2 ± 0.3	2.97 ± 0.48	3.19 ± 0.06	[44]
		10	64.8 ± 1.1	2.36 ± 0.31	4.86 ± 0.23	
		20	73.7 ±1.3	1.94 ± 0.25	6.01 ± 0.26	
		30	80.6 ± 0.9	1.51 ± 0.16	7.09 ± 0.41	
	nanofibrils (CNF)	0	26.1 ± 7.8		2.650 ± 0.0784	[46]
		1	28.3 ± 3.6		2.939 ± 0.168	
		3	43.4 ± 1.8		3.407 ± 0.0995	
		5	34.4 ± 6.1		3.076 ± 0.0958	
	Pine Kraft lignin	0	55.9 ± 0.6	4.6 ± 0.22	2.30 ± 0.04	[15]
		5	50.3 ± 0.9	2.8 ± 0.1	2.33 ± 0.05	
		10	50.1 ± 0.5	2.3 ± 0.17	2.41 ± 0.06	
		15	41.3 ± 0.5	1.9 ± 0.34	2.39 ± 0.06	
	Softwood lignin	0	58.45 ± 0.55	2.5 ± 0.1	2.89 ± 0.014	[47]
		20	39.35 ± 1.05	1.8 ± 0.1	1.46 ± 0.156	
		40	45.65 ± 0.05	1.9 ± 0.08	2.695 ± 0.148	

Figure 33: Table taken from [44], table 3.

3.3.2 Material Extrusion: Thermosets

Subject matter expert Christopher Hershey was consulted in writing this section.

Large scale additive manufacturing with thermosets boasts a few major advantages over thermoplastics: better interlaminar bonding, significantly higher maximum layer time, and finer resolution. Two material systems are currently used on the MVP: one ambient-cured system of vinyl ester and one latent-cured system of epoxy anhydride. A variety of fillers have been used with these materials systems, including clay, carbon fiber, glass fiber, and hollow glass microspheres. Nozzle sizes currently in use on the MVP range from 0.5mm to 0.3in in diameter. Due to the comparatively slow solidification rate of thermosets, thin-walled structures prove challenging to construct. Shrinkage and resultant warping are common issues, however using low-shrink additives or cyclic form thermosets can aid in mitigating shrinkage. The vinyl ester system shrinks more than the epoxy anhydride system. Typical throughput rates are about 15 lb/hr for vinyl ester and 10 lb/hr for epoxy anhydride. The throughput is limited by the pressure required to pump. Overhang angles of about 20 degrees have been printed without problems. In general, larger parts lead to longer layer times, which in part allow for a greater range of overhang geometries. The enhanced interlaminar bonding is seen thanks to chemical crosslinking at the interlaminar interface. Because some thermosets can be used in autoclave, they are particularly attractive for tooling.

The ambient-cured system generates an exotherm as it cures, which can cause liquefaction of prior layers for layer times less than 8 minutes. This material system has been specially formulated as an adhesive, which allows for essentially no maximum layer time. For the vinyl ester material system, thin-walled structures are achievable provided there is adequate layer time. This material system can achieve a bridging distance of 0.85in. In theory overhang angles of 45 degrees are achievable, but these must be carefully weighed with tradeoffs in printing time as layer times of about 30 minutes would be required. One special consideration for the vinyl ester system is its incompatibility with printing small parts. This is because the difference between the reaction time and the layer time is infeasibly large: violating the layer time minimum bound would result in excessive heat accumulation and eventual collapse, while maintaining the minimum layer bound would result in blockages in the nozzle.

The latent-cured system has no minimum layer time. However, the effective maximum layer time is about 2 days, after which continued printing will not have as much interlaminar chemical bonding. For the epoxy anhydride system, an approximate 4:1 ratio is used as a rule of thumb: structures that are 4 times taller than they are wide require additional support. This material system can achieve a bridging distance of 1.4in. Overhangs are more difficult than with the ambient-cured system, as the part buckles or viscoelastic creep leads to sag and failure. One special consideration for the latent-cured system is that parts must be oven cured after the part is built. As such, build size is limited not just by available build space but also by oven size.

3.3.3 DED: mBAAM

Mechanical properties yielded by the mBAAM system are closely linked to the microstructure and porosity of deposited material. Lower porosity leads to higher strength, with some measurements of ultimate and yield tensile strengths of 475 MPa and 375 MPa, respectively. Strength of printed parts may exceed those of conventionally-produced parts thanks to finer microstructures in general [68]. Post-processes such as hot isostatic pressing, heat treatment, and polishing may improve fatigue strength of a part, which is negatively impacted by porosity and layered surface finish.

One major consideration in DED is the lack of **process omnidirectionality** [82]. Process omnidirectionality refers to the ability of the print head to move in any direction in the horizontal plane at any time throughout the process without negatively affecting the print quality. For wire-fed systems in particular, this is not possible and must be considered throughout the design process. The printhead travels toward where the wire enters the melt pool. Thus, quick 180° changes in direction are impossible and machine-specific limitations must be acknowledged.

3.3.4 Binder Jetting: 3DSP

3DSP is typically leveraged to create large sand-casting molds and tools. Thus, design considerations must include both the printing and casting processes [83]. However, AM of the tooling allows for greater geometrical freedom and challenges some traditional casting design rules [84, 85]. For example, rounded edges, undercuts, and datums are easier to implement with 3DSP while draft angles are not required. Maintaining uniform sections at intersections or boss-like features is easier with 3DSP as well. However, constraints of 3DSP include a fixed build volume and minimum feature size. Large castings can be subdivided into multiple pieces for later assembly. Special attention should be given to wall-to-wall thicknesses and holes—which must be no smaller than the minimum feature size of the system. Additionally, high aspect ratio features and long, unsupported, thin walls should be avoided due to the fragility of “green” parts.

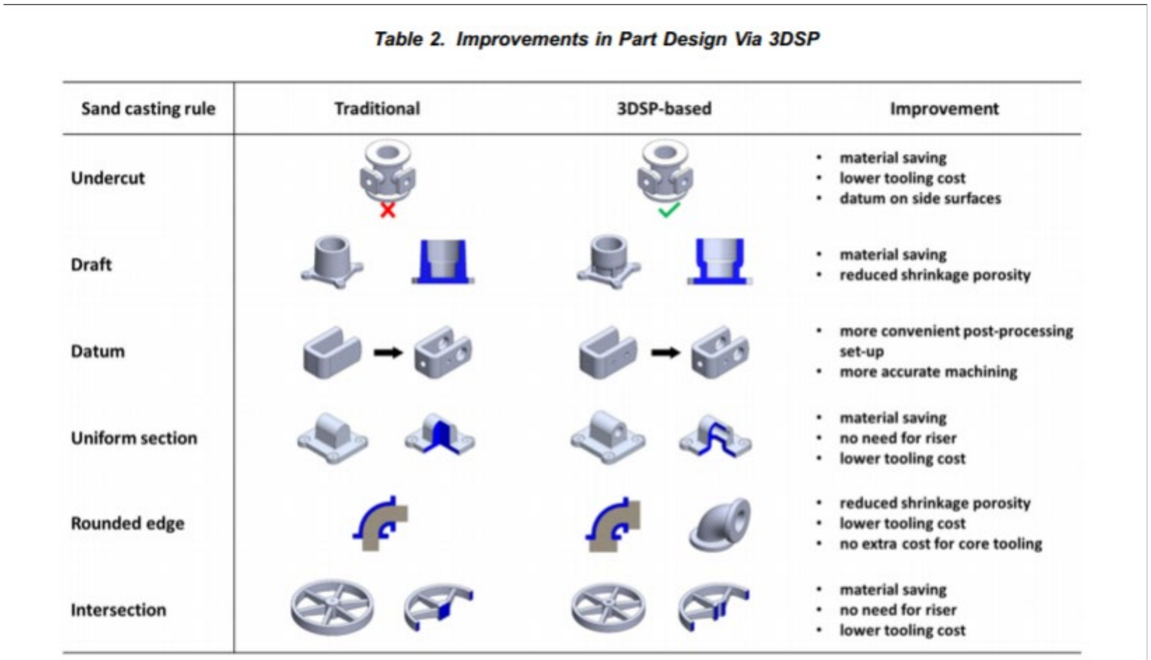

Table 2. Improvements in Part Design Via 3DSP

Sand casting rule	Traditional	3DSP-based	Improvement
Undercut			• material saving • lower tooling cost • datum on side surfaces
Draft			• material saving • reduced shrinkage porosity
Datum			• more convenient post-processing set-up • more accurate machining
Uniform section			• material saving • no need for riser • lower tooling cost
Rounded edge			• reduced shrinkage porosity • lower tooling cost • no extra cost for core tooling
Intersection			• material saving • no need for riser • lower tooling cost

Figure 34. Table of design guidelines from [83]

3DSP casting techniques are still subject to traditional design for casting rules regarding casting defects and post-processing: machining allowance, uniform sections, wall thickness, rounded edges, and so on. In general, considerations for smooth, laminar flow to evenly fill the cavity of the mold should be taken, as well as rapid and uniform cooling to decrease cycle time and warpage and account for material shrinkage. To achieve smooth, laminar flow and reduce shrink cavity development, sharp corners or large variations to wall thickness should be avoided. Large variations in wall thicknesses leads to large variations in cooling rate, which can cause warpage. Additionally, thick regions are prone to develop hot spots which lead to internal voids or porosity that compromise end part strength [34]. In general Chvorinov’s rule should be considered: the solidification time is directly proportional to the square of the volume-to-area ratio of the casting section. Further detail and explanation on traditional casting design rules and methods can be found in the ASM Handbook on Design for Casting [86] or similar. Examples of cast parts from 3D printed sand molds include work by Snelling et. al. [87] as well as Post et. al. [88]. Prior to Snelling’s work, Meisel et. al. [89] attempted similar geometry but encountered unfilled spaces in truss arms, which they attributed to trapped gases during the mold pouring process. Snelling investigated this hypothesis in [90], where different binder systems were compared for burnout characteristics and strengths. Careful consideration of material selection for printed sand-casting molds is paramount to leveraging the geometric advantages that additive manufacturing offers.

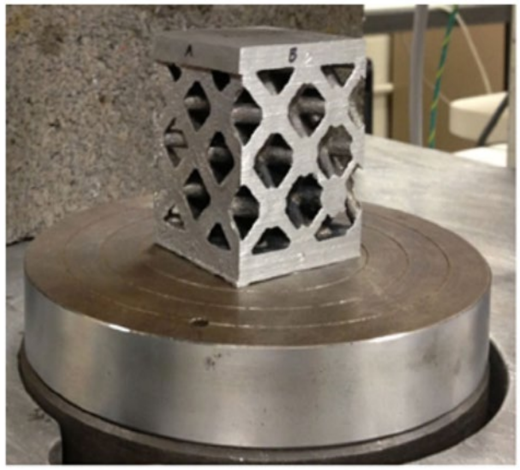

Figure 35. Cast part from printed sand mold [87].

Figure 36. Cast part from printed sand mold [88].

4. CONCLUSION

While additive manufacturing techniques do not currently represent a cure-all to every manufacturing challenge that wind designers face, these techniques and processes present unique advantages to their conventional counterparts that may, with further research and development, lead to innovative solutions for the wind industry. As the scale of wind turbines and their constituent components continues to increase, the need to leverage advanced manufacturing methods such as additive manufacturing will grow in tandem. This document has described the seven families of additive manufacturing, down-selected to those families that are most apt to large-scale applications, and detailed important considerations and limitations of these processes. Further research and development opportunities to explore and apply these processes to wind turbine applications may build upon this work.

5. REFERENCES

[1] S. Yao *et al.*, "Aero-structural design and optimization of 50 MW wind turbine with over 250-m blades," *Wind Engineering,* vol. 46, no. 1, pp. 273-295, 2021, doi: 10.1177/0309524x211027355.

[2] L. Fingersh, M. Hand, and A. Laxson, "Wind Turbine Design Cost and Scaling Model," National Renewable Energy Laboratory, 2006.

[3] R. H. Crawford, "Life cycle energy and greenhouse emissions analysis of wind turbines and the effect of size on energy yield," *Renewable and Sustainable Energy Reviews,* vol. 13, no. 9, pp. 2653-2660, 2009, doi: 10.1016/j.rser.2009.07.008.

[4] C. Desmond, J. Murphy, L. Blonk, and W. Haans, "Description of an 8 MW reference wind turbine," *Journal of Physics: Conference Series,* 2016, doi: 10.1088/1742-6596/753/9/092013.

[5] E. Gaertner *et al.*, "Definition of the IEA 15-Megawatt Offshore Reference Wind," IEA Wind, 2020.

[6] H. Bredmose *et al.*, "Definition of the 15MW Reference Wind Turbine," COREWIND, 2020.

[7] J. Peeringa, R. Brood, O. Ceyhan, W. Engels, and G. d. Winkel, "Upwind 20MW Wind Turbine Pre-Design: Blade design and control," Energy Research Centre of the Netherlands, 2011.

[8] C. E. S. d. Souza and E. E. Bachynski-Polić, "Design, structural modeling, control, and performance of 20 MW spar floating wind turbines," *Marine Structures,* vol. 84, 2022, doi: 10.1016/j.marstruc.2022.103182.

[9] T. Ashuri, J. R. R. A. Martins, M. B. Zaaijer, G. A. M. van Kuik, and G. J. W. van Bussel, "Aeroservoelastic design definition of a 20 MW common research wind turbine model," *Wind Energy,* vol. 19, no. 11, pp. 2071-2087, 2016, doi: 10.1002/we.1970.

[10] E. Stehouwer and G. J. v. Zinderen, "Conceptual nacelle designs of 10-20 MW wind turbines," INNWIND.EU, 2016.

[11] A. Roschli, M. Borish, C. Lai, and B. Post, "The Fundamentals of Slicing for Extrusion-Based Additive Manufacturing."

[12] "7 Families of Additive Manufacturing," ed: Hybrid Manufacturing Technologies.

[13] *ISO/ASTM 52910 Additive manufacturing — Design — Requirements, guidelines and recommendations*, ISO/ASTM, 2018.

[14] "Formlabs Material Library," Formlabs, 7/4/2020 2020.

[15] "Formlabs Materials Library," Formlabs, Q1 2021 2021.

[16] J. R. Tumbleston *et al.*, "Continuous liquid interface production of 3D objects," *Science,* vol. 347, no. 6228, pp. 1349-1352, 2015, doi: 10.1126/science.aaa2397.

[17] "SLA vs PolyJet: What You Need to Know." https://www.cadimensions.com/sla-vs-polyjet-need-know/ (accessed 2021).

[18] "Stereolithography (STL) Fact Sheet." [Online]. Available: https://www.3dsystems.com/resources/information-guides/stereolithography/sla

[19] C. B. Williams and L. B. Bezek, "Material Jetting of Polymers," in *Additive Manufacturing Processes*, 2020, pp. 58-68.

[20] M. Vaezi, P. Drescher, and H. Seitz, "Beamless Metal Additive Manufacturing," *Materials (Basel),* vol. 13, no. 4, Feb 19 2020, doi: 10.3390/ma13040922.

[21] F. Fischer, "FDM and PolyJet 3D Printing," Stratasys. Accessed: 3/22/2021.

[22] "FDM and PolyJet 3D Printing."

[23] "Objet260 Connex3." [Online]. Available: https://prototypingsolutions.com/printers/production-series/objet-connex3/

[24] B. O'Neal. "MakerJuice's WaxCast Resin Offers New Opportunity for Jewelry Makers & SLA 3D Printing." 3DPrint.com. https://3dprint.com/126645/makerjuice-waxcast-resin/ (accessed.

[25] "Material Jetting (PolyJet) 3D Printing: Everything You Need To Know." 3dsourced. https://www.3dsourced.com/guides/polyjet/#PolyJet_Material_Jetting_Materials (accessed 2021).

[26] "Comparing AM Processes." http://apt.mit.edu/am-process-comparisons (accessed 2021).

[27] A. Elliott and C. Waters, *Additive Manufacturing for Designers: A Primer*. 2019.
[28] A. Paolini, S. Kollmannsberger, and E. Rank, "Additive manufacturing in construction: A review on processes, applications, and digital planning methods," *Additive Manufacturing,* vol. 30, 2019, doi: 10.1016/j.addma.2019.100894.
[29] "Economics of Metal Additive Manufacturing." Digital Alloys. https://www.digitalalloys.com/blog/economics-metal-additive-manufacturing/ (accessed 2021).
[30] "Comparing Sand-Additive Costs Per Mixed Ton." Foundry Mag. https://www.foundrymag.com/ask-the-expert/article/21928749/comparing-sandadditive-costs-per-mixed-ton (accessed 2021).
[31] P. R. Carey and M. Lott, "Sand Binder Systems," Ask-Chemicals.
[32] C. B. Williams, J. K. Cochran, and D. W. Rosen, "Additive manufacturing of metallic cellular materials via three-dimensional printing," *The International Journal of Advanced Manufacturing Technology,* vol. 53, no. 1-4, pp. 231-239, 2010, doi: 10.1007/s00170-010-2812-2.
[33] "Metal Binder Jetting." Digital Alloys. https://www.digitalalloys.com/blog/binder-jetting/#:~:text=Binder%20Jetting%20OEMs%20advertise%20a,to%2012%2C000%20cc%2Fhr%E2%80%9D. (accessed 2021).
[34] "ExOne Sand Binder Jet 3D Printing," 2020.
[35] S. Vock, B. Klöden, A. Kirchner, T. Weißgärber, and B. Kieback, "Powders for powder bed fusion: a review," *Progress in Additive Manufacturing,* vol. 4, no. 4, pp. 383-397, 2019, doi: 10.1007/s40964-019-00078-6.
[36] D. B. Mueller *et al.*, "Design for Additive Manufacturing: Guidelines and Case Studies for Metal Applications," presented at the TraCLight workshop, Waterloo.
[37] "Powder Bed Fusion (PBF)." Digital Alloys. https://www.digitalalloys.com/blog/powder-bed-fusion/ (accessed 2021).
[38] T. Gutowski *et al.*, "Note on the Rate and Energy Efficiency Limits for Additive Manufacturing," *Journal of Industrial Ecology,* 2017.
[39] "Benefits of Wire vs. Powder Metal 3D Printing." https://www.sciaky.com/additive-manufacturing/wire-vs-powder (accessed 2021).
[40] B. K. Post *et al.*, "Additive Manufacturing of Polyurethane Foam Mold Tooling," February 28, 2019 2019.
[41] S. Kim *et al.*, "Graded Infill Structure of Wind Turbine Blades Accounting for Internal Stress in Big Area Additive Manufacturing," in *CAMX*, Dallas, TX, 2018.
[42] J. Lindahl, C. Hershey, V. Kunc, G. Gladysz, V. Mishra, and K. Shah, "Additive Manufacturing Using Epoxy and Anhydride Curatives," February 4th, 2019 2019.
[43] X. Zhao *et al.*, "Poplar as Biofiber Reinforcement in Composites for Large-Scale 3D Printing," *ACS Applied Bio Materials,* vol. 2, no. 10, pp. 4557-4570, 2019, doi: 10.1021/acsabm.9b00675.
[44] M. E. Lamm *et al.*, "Material Extrusion Additive Manufacturing of Wood and Lignocellulosic Filled Composites," *Polymers (Basel),* vol. 12, no. 9, Sep 17 2020, doi: 10.3390/polym12092115.
[45] P. Chesser *et al.*, "SkyBAAM Large-Scale Fieldable Deposition Platform System Architecture," presented at the Solid Freeform Fabrication Symposium, Austin, Texas, 2019.
[46] J. Gonzalez-Gutierrez, S. Cano, S. Schuschnigg, C. Kukla, J. Sapkota, and C. Holzer, "Additive Manufacturing of Metallic and Ceramic Components by the Material Extrusion of Highly-Filled Polymers: A Review and Future Perspectives," *Materials (Basel),* vol. 11, no. 5, May 18 2018, doi: 10.3390/ma11050840.
[47] J. M. Justino Netto and Z. d. C. Silveira, "Design of an Innovative Three-Dimensional Print Head Based on Twin-Screw Extrusion," *Journal of Mechanical Design,* vol. 140, no. 12, 2018, doi: 10.1115/1.4041175.
[48] L. Love, B. Post, V. Kunc, and A. Roschli, "Commercialization of Big Area Additive Manufacturing," 2020.
[49] A. Roschli *et al.*, "Increasing interlaminar strength in large scale additive manufacturing," presented at the 29th International Solid Freeform Fabrication Symposium, Austin, Texas, 2018.

[50] B. K. Post, R. F. Lind, P. D. Lloyd, V. Kunc, J. M. Lindhal, and L. J. Love, "The Economics of Big Area Additive Manufacturing," presented at the International Solid Freeform Fabrication Symposium, Austin, Texas, 2016.
[51] D. L. Bourell, J. J. Beaman, and T. Wohlers, "History and Evolution of Additive Manufacturing," in *Additive Manufacturing Processes*, 2020, pp. 11-18.
[52] D. L. Bourell and T. Wohlers, "Introduction to Additive Manufacturing," in *Additive Manufacturing Processes*, 2020, pp. 3-10.
[53] B. Richardson *et al.*, "The current state of additive manufacturing in wind energy systems," in "ORNL Report," 2017, vol. ORNL/TM-2017/479.
[54] G. Costabile, M. Fera, F. Fruggiero, A. Lambiase, and D. Pham, "Cost models of additive manufacturing: A literature review," *International Journal of Industrial Engineering Computations,* pp. 263-283, 2017, doi: 10.5267/j.ijiec.2016.9.001.
[55] D. Thomas, "Costs, Benefits, and Adoption of Additive Manufacturing: A Supply Chain Perspective," *International Journal of Advanced Manufacturing,* 2015.
[56] A. J. Pinkerton, "Lasers in Additive Manufacturing," *Optics and Laser Technology,* vol. 78, 2015, doi: http://dx.doi.org/10.1016/j.optlastec.2015.09.025.
[57] M. Baumers, "Economic aspects of additive manufacturing: benefits, costs and energy consumption," Loughborough University, 2012.
[58] D. S. Thomas and S. W. Gilbert, "Costs and Cost Effectiveness of Additive Manufacturing: A Literature Review and Discussion," NIST, 2014.
[59] A. Roschli *et al.*, "Designing for Big Area Additive Manufacturing," *Additive Manufacturing,* vol. 25, pp. 275-285, 2018 2018, doi: 10.1016/j.addma.2018.11.006.
[60] C. Greer *et al.*, "Introduction to the design rules for Metal Big Area Additive Manufacturing," *Additive Manufacturing,* vol. 27, no. N/A, pp. 159-166, 2019 2019, doi: 10.1016/j.addma.2019.02.016.
[61] J. Etienne *et al.*, "CurviSlicer: Slightly curved slicing for 3-axis printers," *ACM Transactions on Graphics,* vol. 38, no. 4, pp. 1-11, 2019, doi: 10.1145/3306346.3323022.
[62] A. Roschli, B. Post, P. Chesser, M. Borish, L. Love, and S. Kim, "Creating Toolpaths without Starts and Stops for Extrusion-based systems," presented at the Solid Freeform Fabrication, Dallas, TX, 2019.
[63] I. B. Ishak, "A Robot FDM Platform for Multi-Plane and 3D Lattice Structure Printing," PhD in Mechanical Engineering, Florida Institute of Technology, 2018.
[64] D. Cormier and P. Poddar, "Durability of Composite Systems," K. L. Reifsnider Ed.: Woodhead Publishing, 2020, ch. 12 - Durability of polymer matrix composites fabricated via additive manufacturing, pp. 403-438.
[65] D. Ahlers, "3D Printing of Nonplanar Layers for Smooth Surface Generation," Masters, Universitat Hamburg, 2018.
[66] P. Chesser *et al.*, "Extrusion control for high quality printing on Big Area Additive Manufacturing (BAAM) systems," *Additive Manufacturing,* vol. 28, pp. 445-455, 2019, doi: 10.1016/j.addma.2019.05.020.
[67] Cincinnati Incorporated, "Design Guidelines for BAAM," ed: Cincinnati Inc., 2019, pp. http://wwwassets.e-ci.com/PDF/Products/BAAM-Design-Guidelines.pdf.
[68] B. Shassere, A. Nycz, M. Noakes, C. Masuo, and N. S. Niyanth, "Correlation of microstructure and mechanical properties of metal big area additive manufacturing," *Applied Sciences,* vol. 9, no. 4, p. 787, 2019, doi: 10.3390/app9040787.
[69] A. Messing, A. Roschli, B. K. Post, and L. J. Love, "Using skeletons for void filling in large-scale Additive Manufacturing," presented at the International Solid Freeform Fabrication Symposium, Austin, Texas, 2017.
[70] A. Roschli, B. K. Post, P. C. Chesser, M. Sallas, L. J. Love, and K. T. Gaul, "Precast concrete molds fabricated with big area additive manufacturing," 2018.

[71] L. J. Love *et al.*, "Feasibility of Using BAAM for Mold Inserts for the Precast Concrete Industry," 2019.
[72] B. K. Post *et al.*, "Using Big Area Additive Manufacturing to directly manufacture a boat hull mould," *Virtual and Physical Prototyping,* vol. 14, no. 2, pp. 123-129, 2018, doi: 10.1080/17452759.2018.1532798.
[73] S. Curran *et al.*, "Big Area Additive Manufacturing and Hardware-in-the-Loop for Rapid Vehicle Powertrain Prototyping: A Case Study on the Development of a 3-D-Printed Shelby Cobra," presented at the SAE World Congress, Detroit, MI, 2016.
[74] L. Love, B. K. Post, and A. Roschli, "Wide and High Additive Manufacturing (WHAM)," 2017.
[75] C. Duty *et al.*, "Z-pinning approach for reducing mechanical anisotropy of 3D printed parts," presented at the Solid Freeform Fabrication, 2018.
[76] P. C. Chesser, R. F. Lind, B. K. Post, A. Roschli, L. J. Love, and K. T. Gaul, "Using Post-tensioning in large scale additive manufacturing parts for load bearing structures," presented at the 29th Annual International Solid Freeform Fabrication Symposium, Austin, Texas, 2018.
[77] X. Zhao *et al.*, "High-Strength Polylactic Acid (PLA) Biocomposites Reinforced by Epoxy-Modified Pine Fibers," *ACS Sustainable Chemistry & Engineering,* vol. 8, no. 35, pp. 13236-13247, 2020, doi: 10.1021/acssuschemeng.0c03463.
[78] H. L. Tekinalp *et al.*, "High modulus biocomposites via additive manufacturing: Cellulose nanofibril networks as “microsponges”," *Composites Part B: Engineering,* vol. 173, 2019, doi: 10.1016/j.compositesb.2019.05.028.
[79] J. Burke, "Manufacturing - Recycling goes large," in *Oak Ridge National Laboratory News*, ed, 2021.
[80] H. L. Tekinalp *et al.*, "Additive Manufacturing of Lightweight Structures: Microfibrillated Cellulose – PLA Biofoams," presented at the CAM-X 2021, Dallas, TX, 2021.
[81] H. L. Tekinalp, D. Ker, B. Benson, V. Kunc, W. Peter, and S. Ozcan, "Micro-cellulose fibre reinforced biocomposites for additive manufacturing," presented at the CAMX – The Composites and Advanced Materials Expo, Dallas, Texas, 2018.
[82] A. Nycz, M. Noakes, and M. Cader, "Additive Manufacturing - A New Challenge for Automation and Robotics," in *Automation*, 2018 2018, Cham: Springer International Publishing, pp. 3-13, doi: 10.1007/978-3-319-77179-3_1.
[83] J. Wang, S. R. Sama, and G. Manogharan, "Re-Thinking Design Methodology for Castings: 3D Sand-Printing and Topology Optimization," *International Journal of Metalcasting,* vol. 13, no. 1, pp. 2-17, 2019/01/01 2019, doi: 10.1007/s40962-018-0229-0.
[84] N. Hawaldar and J. Zhang, "A comparative study of fabrication of sand casting mold using additive manufacturing and conventional process," *The International Journal of Advanced Manufacturing Technology,* vol. 97, no. 1-4, pp. 1037-1045, 2018, doi: 10.1007/s00170-018-2020-z.
[85] M. Upadhyay, T. Sivarupan, and M. E. Mansori, "3D printing for rapid sand casting-A review " *Journal of Manufacturing Processes, Society of Manufacturing Engineers,* vol. 29, pp. 211-220, 2017, doi: 10.1016/j.jmapro.2017.07.017.
[86] T. S. Piwonka, "Design for Casting," in *Materials Selection and Design*, G. E. Dieter Ed.: ASM International, 1997, pp. 723-729.
[87] D. Snelling, Q. Li, N. Meisel, C. B. Williams, R. C. Batra, and A. P. Druschitz, "Lightweight Metal Cellular Structures Fabricated via 3D Printing of Sand Cast Molds," *Adv Eng Mater,* vol. 17, no. 7, pp. 923-932, 2015, doi: 10.1002/adem.201400524.
[88] B. K. Post *et al.*, "A Comparative Study of Direct and Indirect Additive Manufacturing Approaches for the Production of a Wind Energy Component," 2021.
[89] N. A. Meisel, C. B. Williams, and A. Druschitz, "Lightweight Metal Cellular Structures via Indirect 3D Printing and Casting," presented at the 23rd Annual International Solid Freeform Fabrication Symposium, 2012.

[90] D. Snelling, C. Williams, and A. Druschitz, "A Comparison of Binder Burnout and Mechanical Characteristics of Printed and Chemically Bonded Sand Molds," presented at the Solid Freeform Fabrication, UTEP, 2014.